Best Practice in RSS Measurements and Ranging

Andrea Zanella, *Senior Member, IEEE*

***Abstract*—The term "ranging" is often used to indicate the operations that make it possible to estimate the distance between two nodes by processing some signals generated and/or received by the nodes. In wireless systems, a very popular ranging method makes use of the radio signal strength (RSS), which is a measure of the received radio signal power. However, RSS-based ranging is considered very inaccurate, particularly in indoor environments, mainly because of the randomness of the received signal power. In this tutorial paper, we provide an in-depth analysis of the main factors that affect the variability of the received signal power and the accuracy of the RSS measurements. Starting from a survey of the most common and widely accepted models for the radio signal propagation and the RSS-based ranging, we then focus our attention on some technological and procedural pitfalls that are often overlooked, but may significantly affect the accuracy of the RSS-based ranging, and we suggest possible techniques to alleviate such problems. The theoretical argumentation is backed up by a set of empirical results in different scenarios. We conclude this paper by providing some best-practice recommendations for proper RSS-based ranging estimation in wireless networks and discussing new approaches and open research challenges.**

***Index Terms*—Communications technology, radio signal strength, RSS, RSSI, ranging, indoor, outdoor, localization, measurements, 802.15.4, zigbee.**

I. Introduction

THE VAST majority of today's wireless transceivers offers the possibility of measuring the so-called *Radio Signal Strength* (RSS), i.e., the power (or energy) of the received radio signal. This information can be profitably used in many different ways and for a variety of applications. As a consequence, the collection and processing of RSS measurements have gathered huge interest and produced a steady and conspicuous stream of publications in the last decade. To have a rough idea of the popularity of the topic, it suffices to query the IEEE Xplore digital library[1] for the documents that have "RSS" or "RSSI"[2] in their *Index Terms* to get thousands of hits, out of which, several hundreds published in the last two years.

A quick survey of applications based on RSS measurements in wireless systems are given in Section II. A very important and popular class of applications is that for the *localization and tracking* of wireless nodes in a certain area [1]. Although the literature on RSS-based localization is extremely wide and variegate, a first rough classification can be made in terms of *range-free* [2] and *range-based* [3] algorithms.

Range-free methods do not use the RSS values to infer the distances among the nodes, but rather consider connectivity or signal propagation aspects (see, e.g., the surveys [4], [5], or the papers [6]–[14]).

Range-based approaches, on the other hand, make use of distance estimates obtained by processing signals exchanged by the nodes, an operation that is commonly referred to as *ranging*. Once a sufficient number of range estimates between pairs of nodes have been collected, it is possible to estimate the nodes position in the area by using multilateration algorithms [15], [16], semidefinite programming [17]–[19], maximum likelihood estimators [20], [21], or spring-mass relaxation approaches [22]–[24].

Common ranging techniques are based on the measurement of the *time of flight* (TOF) of acoustic [25], light [26], or radio frequency (RF) [27], [28] signal pulses. The TOF of a pulse is the time taken by the signal to cover the distance that separates transmitter and receiver. Knowing the propagation speed of the signal in the considered environment, it is then possible to estimate the distance between transmitter and receiver.

The accuracy of this method, however, is limited by the precision of the time-synchronization between the transmitter and the receiver, and by the echo phenomena. The first issue can be counteracted by using pair-wise ranging techniques, in which the signal impulse received by a node is immediately echoed back to the source, which then measures the *round-trip time of flight* [29]. Yet another method, based on the *difference of time of flight* (DTOF), consists in measuring the propagation time of two signal pulses of different nature, usually RF and acoustic, which are simultaneously emitted by the transmitter, but separated by a time interval Δ_t at the receiver because of the very different propagation speeds. Neglecting the propagation time of the RF impulse, the distance between the nodes can then be estimated as $\hat{d} = v_2 \Delta_t$, where v_2 is the speed of the acoustic pulse in air [30].

Overall, RF-based TOF ranging remains quite critical in indoor environments, because of the short distances to be estimated and the multipath distortion of the transmitted signals that may undergo several reflections and obstructions before reaching the receiver. On the other hand, acoustic-based TOF methods generally achieve quite good performance, but require ancillary hardware and more energy [31].

In this scenario, the *RSS-based ranging* techniques are particularly attractive because of their intrinsic simplicity, the

Manuscript received August 6, 2015; revised March 1, 2016; accepted April 8, 2016. Date of publication April 12, 2016; date of current version November 18, 2016.

The author is with the Department of Information Engineering, University of Padova, Padova 35131, Italy (e-mail: zanella@dei.unipd.it).

Digital Object Identifier 10.1109/COMST.2016.2553452

[1] http://ieeexplore.ieee.org

[2] The acronym RSSI stands for *Radio Signal Strength Indicator* and refers to the integer value typically in the range {0, 255}, provided by many commercial wireless transceivers in place of the actual value (in dBm) of the received signal power, according to a given power-to-RSSI transduction law. In the following of this paper, we will use the acronym RSS also with reference to RSSI.

native support for RSS measurements provided by the most common wireless transceivers (TmoteSky, TelosB, MicaZ, Imote2, and so on), and the possibility to get RSS measurements from standard data packet traffic, without any additional energy expenditure.

The underlying assumption of the RSS-based ranging is that the average power of a radio signal decays with the distance from the transmitter according to some deterministic attenuation law, generally referred to as *Path-Loss Model* (PLM). Knowing the PLM, it is hence possible to invert the propagation law to map the RSS measured at the receiver into an estimate of the distance from the transmitter [32].

Despite its wide popularity, RSS is often reckoned to be inappropriate for accurate ranging, particularly in indoor environments where the random factors that affect the radio signal propagation may yield unpredictable received power values, which make the RSS-based ranging quite unreliable [23], [33], [34]. Notwithstanding this (or, perhaps, because of this), the subject has collected huge interest and produced a steady and conspicuous stream of publications in the last decade.

For example, a software-defined tool based on the universal radio peripheral (USRP) with GNU software for experimenting with RSS measurements in IEEE 802.15.4 networks is proposed in [35]. An experimental study of the RSS measurements and the RSS-based ranging in outdoor scenarios is carried out in [36]. Interestingly, the paper proves that the RSS-based ranging can provide reasonable localization performance in outdoor environments but, at the same time, reveals the fragility of the approach, which is extremely sensitive to the environmental conditions and the experimental settings. Another source of errors that is seldom considered in the RSS-based localization literature is the attenuation produced by the human body and the hand grip on the device. An experimental evaluation of human-induced perturbations on the RSS measurements can be found in [37], where the authors show that both hand-grip and body-loss can severely compromise the accuracy of the RSS-based ranging, even when cooperative localization schemes are used. On the other hand, they experimentally demonstrate that these human-related impairments can not only be mitigated, but even exploited to improve the performance of cooperative localization algorithms, if correctly understood and accounted for. However, this requires a deep knowledge and characterization of the application scenario and the access to ancillary signals, such as the orientation of the devices, which may not always be feasible. A complete survey of such a huge body of literature, however, is out of the scope of this manuscript, and the reader interested on a more thorough introduction of the subject is referred to the literature, where there are a number of excellent survey papers as, for instance, [5], [31], [38]–[42].

The purpose of this tutorial paper, instead, is to provide a *digest of the best-practice guidelines for RSS measurements and RSS-based ranging*. In this tutorial paper, we systematically analyse and revise the typical steps involved in the RSS-based ranging, and we provide practical suggestions to improve the quality of the RSS measurements and, in turn, the accuracy of the RSS-based ranging.

We hence address the matter of the RSS-based ranging by providing an in-depth analysis of the main factors that affect the variability of the received signal power and the accuracy of the RSS measurements. Starting from a survey of the most common and widely accepted models of radio signal propagation and RSS-based ranging, we then focus our attention on some technological and methodological pitfalls that are often overlooked, but may significantly affect the accuracy of RSS-based ranging, and we discuss possible counteractions. To support our claims, we present a set of empirical results collected in different scenarios by using TmoteSky nodes, whose MAC and PHY layers are compatible with the IEEE 802.15.4 standard, as well as other data publicly available in the Internet.

Although most of the aspects discussed in the paper have general validity, the study is mainly focused on indoor scenarios. The reason for this choice is twofold: first, indoor RSS-based ranging is generally more challenging than outdoor, because of the harsher wireless signal propagation; therefore greater benefit is expected by the proper handling of the RSS measurement process. Second, the radio transceivers of indoor wireless devices are generally cheaper than that of outdoor devices, both in terms of cost and manufacturing, so that the RSS measurements collected by indoor wireless devices are more likely affected by the device-dependent artefacts that will be discussed in the paper. Nonetheless, we remark that most of the best practice methodologies referenced in this paper generally apply to both indoor and outdoor RSS measurements, though with possibly minor impact in the second case. For the sake of completeness, we also report some outdoor RSS measurements and discuss similarities and differences with the RSS measurements typically collected in indoor environments.

The rest of the paper is organized as follows. Section II briefly surveys common applications based on RSS measurements and/or ranging. The following three sections are of service for the remaining of the argumentation. More specifically, Section III introduces the main notation of the paper, Section IV defines the reference mathematical framework for the RSS measurements and the RSS-based ranging, and the models and methodologies which are at the core of the study, while Section V illustrates the hardware and the various experimental scenarios that have been used to substantiate the theoretical argumentation. Then, we will address one by one the fundamental steps involved in the RSS-based ranging: Section VI deals with the issues regarding the calibration of the RSS circuit; Section VII discusses the reduction of short-term variations in the RSS readings by averaging multiple RSS samples collected in different time instants; Section VIII addresses the estimate of the PLM parameters; and Section IX analyzes the technical and methodological pitfalls that may increase the variability of the RSS measurements and, in turn, worsen the accuracy of the RSS-based ranging.

The effects of the methodologies discussed in the previous sections are illustrated in Section X by using mainly indoor experimental RSS measurements, while Section XI discusses other scenarios, such as outdoor, non line-of-sight, and so on.

Finally, Section XII concludes the paper by drawing some final remarks and discussing open research challenges.

II. Applications

This section provides a quick overview of some representative applications that make use of RSS measurements for different purposes.

As mentioned in the introduction, a first, important use of the RSS measurements is to perform some sort of ranging. This type of application assumes that the radio signal strength decreases progressively with the distance from the transmitter. As we will see in the next sections, this deterministic relation between received power and distance is often spoiled by the "noise" that affects the RSS measurements, originated by the propagation conditions of the environment and the peculiarities of the wireless equipment used to collect the measurements. Nonetheless, the RSS-based ranging has been largely used in the literature, and even in commercial applications, with some satisfaction.

An example is offered by the *proximity services*, which associate the reception of a sufficiently strong radio signal (e.g., LTE, Bluetooth) to the presence of a node within a limited distance from the receiver [43], [44], thus enabling proximity marketing applications, such as local advertising, distribution of media at malls/concerts/exhibitions, information at airports or open fairs, gaming, social applications, and so on.

Another ranging-based application is the *symbolic localization*, whose goal is to identify the location of the node within predefined areas in a map (e.g., a room in a building, or a specific location in a grid), rather than the exact geographical position of the node [5], [45]. The symbolic localization is useful, for example, to find people in a large building or at a conference, to locate the deposit area of a certain good in a wide warehouse, to automatically associate antitheft devices to the art pieces in a museum, or to find the place occupied by a certain soil-monitoring sensor in a regular pattern of sensors placed in a greenhouse [46]. In this case, beacons are typically placed within the target location (e.g., rooms), and the RSS samples collected by the mobile node are compared to find the most likely location, still using a proximity principle.

We then have the more classical self-localization algorithms, where the power-distance decay law is inverted to get some (noisy) distance estimates between node and beacons, which are then used to infer the geographical position of the node with respect to the beacons coordinates, using different techniques (see, e.g., [36], [47], [48]). This type of localization is needed whenever the nodes can occupy any position in the area as, for example, in the case of random deployment of environmental sensors in a field to be monitored, or of tags attached to objects that can be freely placed in the area.

When nodes are mobile, the RSS-based measurements can be used by tracking algorithms, which attempt to estimate the motion of the node in the space by using consecutive RSS readings from the beacons, possibly together with some other types of signal [49]–[52].

A recent and interesting application of the RSS-based ranging is in the Simultaneous Localization and Mapping (SLAM) problem, where the radio signals broadcasted by a number of (smart) objects placed in an unknown environment are used by an autonomous mobile robot to estimate its own position, while simultaneously mapping the position of the objects in the environment. The variability of the RSS measurements is counteracted by using different filtering techniques, such as the Extended Kalman Filter (EKF-SLAM), the Delayed Particle Filter (DPF), and so on [53]–[55]. In [56] and [57], it is also proposed to use the RSS-based SLAM for a first, rough estimate of the object positions in the environment, and then using stereoscopic visual features identification algorithms to finely locate the object in the space. This service may enable the creation of smart environments that can be autonomously navigated by team of service robots for different purposes, e.g., supporting rescue teams in dangerous situations (as exploring burning or unsafe buildings), helping elderly or impaired people in their daily life (assisted leaving), increasing factory automation, and so on.

Another use of the RSS measurements, not related to the distance estimation, regards the assessment of the *radio channel quality*. The basic assumption here is that the stronger the radio signal, the better the reception. Generally speaking, this principle is correct, even though the actual performance of the wireless communication depends on a number of other factors as, for instance, the level of interference, the frequency response of the channel, the capabilities of the receiver. Nonetheless, the RSS is often used as a practical way to measure the channel quality and exploited in different manners. For example, some rate adaptation algorithms change the transmit rate towards a certain node according to the RSS measured from the node, or even reported by the node itself [58]–[63].

Another application is the cell-selection in mobile telecommunication systems, where the RSS measured from different base stations is used by the mobile terminals, possibly with other parameters, to determine the optimal serving cell among those available [64]–[68]. Similarly, the RSS can be used to select the best relay in multi-hop routing algorithms [69], or the best gateway for downlink transmission to remote sensor nodes, as described in the specifications of the emerging Low-power long-Range (LoRa^{TM}) technology [70]–[72]. The RSS measurements can also be used to plan the arrangement of access points in a building or open area, in order to guarantee good radio coverage in every location [73]–[75].

Yet another use of the RSS measurements is as *channel signature*. The underlying idea is to use the vector of RSS samples collected by a node in a certain position from a number of fixed (but not necessarily localized) transmitters as a unique feature of the receiver position, thus exploiting the space variability of the received signal power. Once a (multidimensional) RSS map of the area is available, it is possible to localize a target node by applying the so-called *fingerprinting* methods, which consist in searching the RSS database for the sampling position with the closest RSS signature to that measured by the target node [11]. Evolutions of this approach include the use of statistical and machine-learning methods for position extrapolation [12], [13].

TABLE I
NOTATION

Symbol	Meaning
m_X, σ_X^2, $f_X(\cdot)$	Mean, variance, and PDF of the random variable X
$X(t, \mathbf{s})$, $\bar{X}(\mathbf{s})$	Space-time dependent process and corresponding space dependent time-averaged process
$\hat{X}$	Estimate of the parameter X
P_{tx}	Transmit signal power
G_{tx}, G_{rx}, G	Transmitter, Receiver, Total antenna gain
$\mathbf{s}$	Transmitter-receiver geographical position
ξ	Conversion constant equal to $10\log(e)$
$P_{rx}(t, \mathbf{s})$	Received power at time t in position $\mathbf{s}$ (eq. (2))
$\bar{P}_{rx}(\mathbf{s})$	Time-averaged received power with nodes in position $\mathbf{s}$ (eq. (5))
$\bar{\mathcal{P}}_{rx}(d)$	Random variable modeling the time-averaged received power at distance d (eq. (6))
P_{obs}	A measured received signal power value
$\rho(t, \mathbf{s})$	Received RSS (eq. (1))
$\mathcal{R}(x)$	Actual power-to-RSS mapping function (eq. (1))
$\mathcal{R}_o(x)$	Nominal power-to-RSS transduction law (eq. (17))
c_j	RSS offset of node j (eq. (17))
$\mathbf{R}$	Vector of time-averaged RSS samples (eq. (19))
$\mathbf{p}$	Vector of PLM parameters (eq. (19))
$\hat{\mathbf{p}}$	Vector of PLM estimated parameters (eq. (21))
$\mathbf{X}$	Matrix of log-distance values used for PLM parameters estimation (eq. (20))
$D(d)$	Path-loss at distance d (eq.s (3)–(4))
$D_{inv}(d)$	Inverse function of $D(\cdot)$ (eq. (9))
$\mathcal{K}$	Path-loss constant (eq.s (3)–(4))
η_h, δ_h	Path-loss propagation coefficients and breaking points in multi-slope piece-wise linear PLM (eq. (4))
η, δ_0	Path-loss propagation coefficient and reference distance for single-slope PLM (eq. (3))
a	Short-term (fast) fading process
$a(t)$	A realization of the fast fading at time t
Ψ	Long-term (slow) fading process
μ, σ	Parameters of the lognormal distribution
$\Psi(\mathbf{s})$	A realization of the long-term fading at position $\mathbf{s}$
$\hat{d}(P_{obs})$	MLE of the distance for an average received power P_{obs}
$\hat{d}_{rnd}$	Random variable that models the MLE of the distance
$\varepsilon(d)$	Absolute ranging error at distance d
$\varepsilon_r(d)$	Relative ranging error at distance d
$\varepsilon_{rnd}(d)$	Random variable that models the ranging error at distance d

Besides localization, the RSS signatures can also be used to detect events that cause some noticeable variations of the propagation conditions, such as the passage of objects or persons in the monitored area, a technique which is known in the literature as *radio tomographic imaging* [76]. This unobtrusive technique can be used to localize people in indoor and domestic environments, or detect dangerous events (as falls), which is one of the key requirements for ambient assisted living systems [77].

All these applications are negatively affected by errors in the collection and management of the RSS measurements, even though with different degrees of sensitivity. It is therefore of primary importance to understand which are the factors that may degrade the quality of the RSS readings, and which are the possible countermeasures that can be adopted to alleviate their effect. This is the objective of the remaining of the paper.

III. NOTATION

Before plugging into the study of the RSS-based ranging, we need to introduce the main notation adopted in this paper.

The base 10 and natural logarithm of x are denoted by $\log(x)$ and $\ln(x)$, respectively. Quantities that can be represented both in linear and logarithmic scale are denoted with the same symbol, with the addition of the subscript "LN" in the former case, so that, for a generic dimensionless term X, it holds $X = 10\log(X_{LN})$.

The symbol $\mathbf{s}$ indicates the vector of geographical coordinates of a transmitter-receiver pair, while $d = \|\mathbf{s}\|_2$ denotes the Euclidean distance between the nodes. Note that, for ease of writing, in the following we will refer to $\mathbf{s}$ as the *position* of the transmitter/receiver pair.

A quantity X that may change in time and space is indicated as $X(t, \mathbf{s})$, whereas $\bar{X}(\mathbf{s})$ denotes its time average. For ease of notation, the argument $\mathbf{s}$ will be omitted when not necessary. An estimate of X is denoted by $\hat{X}$.

Given a generic random variable X, its Probability Density Function (PDF) is denoted by $f_X(\cdot)$, while the statistical mean and variance are denoted by m_X and σ_X^2, respectively. Note that, since all the processes considered in the paper are supposed to be ergodic (both in time and space), we will freely interchange ergodic and stochastic averages, on a convenience basis.

For reader's convenience, the main notation used in the remaining of the paper has been collected in Tab. I.

IV. RSS MEASUREMENTS AND RANGING MODELS

This section sets the stage for the rest of the paper, introducing the models and methodologies which serve as baseline for the following discussion. More specifically, we introduce some common reference models for the RSS measurements, the wireless propagation channel, and the RSS-based ranging. Furthermore, we summarize the typical phases involved in the RSS-based ranging process.

A. RSS Measurements Model

Given a pair of nodes in position $\mathbf{s}$, set apart by a line-of-sight (LOS) distance $d = \|\mathbf{s}\|_2$, the RSS measured at time t by the receiver can be expressed as

$$\rho(t, \mathbf{s}) = \mathcal{R}(P_{rx}(t, \mathbf{s})), \tag{1}$$

where $P_{rx}(t, \mathbf{s})$ is the actual received power (typically expressed in dBm), and $\mathcal{R}(\cdot)$ is the power-to-RSS transduction law provided by the receiver RSS circuit. Ideally, $\mathcal{R}(P_{rx}(t, \mathbf{s}))$ should be a rescaled version of the actual received power $P_{rx}(t, \mathbf{s})$. In practice, however, this is not generally the case, as it will be discussed in more details in Section VI.

B. Received Power Model

The received power can be generally expressed (in [dBm]) as

$$P_{rx}(t, \mathbf{s}) = D(d) + \Psi(\mathbf{s}) + a(t). \tag{2}$$

In the above expression, the function $D(d)$ accounts for the deterministic component of the received power at distance d

TABLE II
WALL ATTENUATION FACTORS FOR COMMON CONSTRUCTING MATERIALS [80]

Plasterboard wall	3 dB
Glass wall with metal frame	6 dB
Cinder block wall	4 dB
Office window	3 dB
Metal door	6 dB
Metal door in brick wall	12.4 dB

from the transmitter, according with the considered PLM. The terms $\Psi(\mathbf{s})$ and $a(t)$, instead, model the random variations of the received signal power in space and time, respectively. Such variations are generally due to self-interference phenomena produced by multipath signal propagation and are referred to as *fading*. More specifically, the space-dependent term $\Psi(\mathbf{s})$ is named *long-term* (or *slow*) fading process, while the time-dependent component $a(t)$ is called *short-term* (or *fast*) fading process [78], [79].

The most popular models for the three components of the received signal power, namely the PLM, the long-term fading, and the short-term fading, are discussed in the following.

1) Path-Loss Models (PLMs): A common model for $D(d)$ is the *one-slope path-loss propagation model* [78], according to which

$$D(d) = \mathcal{K} - 10\eta \log(d/\delta_0), \forall d \geq \delta_0. \tag{3}$$

In the above equation, δ_0 is the reference distance after which the far-field assumption and, consequently, the PLM are valid; η is the so-called *path-loss coefficient* and reflects the way the signal power decays with the distance d from the transmitter; while the term $\mathcal{K}$ represents the received power at the reference distance δ_0, i.e., $\mathcal{K} = D(d_0)$, and hence collects all constant factors in the propagation law, namely: the transmit power $\mathrm{P_{tx}}$; the transmitter and receiver antenna gains, $\mathrm{G_{tx}}$ and $\mathrm{G_{rx}}$, respectively, and the wall and floor attenuation coefficients, which depend on the constructing materials as reported in Tab. II.

While the one-slope model is adequate in free space propagation, a multi-slope piece-wise linear propagation model appears more suitable in indoor environments and in the presence of strong reflections [78]. In this case, the average received power at distance d is expressed as

$$D(d) = \mathcal{K} - \sum_{h=1}^{m} 10\eta_h \log\left(\frac{\langle d \rangle_{\delta_{h-1}}^{\delta_h}}{\delta_{h-1}}\right), \tag{4}$$

where $\langle X \rangle_a^b = \min\{\max\{X, a\}, b\}$, and $0 < \delta_0 < \delta_1 < \ldots < \delta_m = \infty$. In practice, (4) defines a continuous piece-wise linear function composed of $m+1$ linear segments, with zero slope for $d \leq \delta_0$, and slope η_h in the interval $(\delta_{h-1}, \delta_h]$, $h = 1, \ldots, m$. Clearly, the piece-wise linear model generalizes the single slope model, which is recaptured by considering a single segment, i.e., setting $m = 1$.

Notice that the parameters in (4) generally depend on the specific characteristics of the environment. Therefore, they can either be set according to precomputed tables provided in the literature for typical environments (see, e.g., [78]), or estimated directly from the collected RSS measurements, as explained later in Section VIII. Another possibility consists in deploying a certain number of anchors (transmitters placed in known position) and characterize the coefficients of (4) from the RSS measurements collected *in loco*, as proposed in [81].

2) Short-Term Fading Models: The short-term fading process $a(t)$ is assumed stationary and ergodic. Therefore, it is common practice to reduce its impact by averaging multiple RSS samples over time [20]. Ideally, time averaging yields

$$\bar{\mathrm{P}}_{\mathrm{rx}}(\mathbf{s}) = \lim_{t\to\infty} \frac{1}{T} \int_0^T \mathrm{P}_{\mathrm{rx}}(t, \mathbf{s}) = D(d) + \Psi(\mathbf{s}), \tag{5}$$

where the mean of $a(t)$ gets absorbed by the constant term $\mathcal{K}$ in $D(\cdot)$. Nonetheless, the way the time average is computed may (marginally) affect the performance of the RSS-based ranging, as discussed in Section VII.

3) Long-Term Fading Models: The long-term fading is assumed position-dependent, but almost time invariant, so that it is unaffected by time averaging. This kind of fading is generated by the scattering of the radio signal due to obstacles in the signal path and/or from the self-interference produced by multiple strong reflections of the signal. This term is often referred to as *shadowing* and commonly modeled (in dB scale) as a normal random variable, with zero mean and standard deviation σ_Ψ that typically ranges from 2 dB to 6 dB in indoor environments [78], [82]. Accordingly, the long-term fading coefficient in linear scale, $\Psi_{\mathrm{LN}} = 10^{\Psi/10}$, turns out to be *lognormal* distributed, with parameters $\mu = 0$ and $\sigma^2 = \sigma_\Psi^2/\xi^2$, where $\xi = 10\log(e)$. For this reason, this type of long-term fading model is also referred to as *lognormal shadowing*.

We remark that, in the rest of the paper, the terms long-term fading and shadowing are used interchangeably to refer to the fading components that are position-dependent. In principle, this fading term can be mitigated by changing the position $\mathbf{s}$ of the transmitter/receiver pair, while maintaining fixed their distance $d = \|\mathbf{s}\|_2$. For example, a pair of nodes that move by maintaining the same reciprocal distance (e.g., sensors attached to a rigid but mobile robotic arm) can collect multiple RSS readings on different locations and average them out to alleviate the influence of the space-dependent fading term, thus obtaining a better estimate of the signal power attenuation due only to the distance d. Unfortunately, this kind of "space averaging" is not feasible in many practical scenarios, so that the effect of the long-term fading cannot usually be eliminated or even attenuated.

C. Path-Loss Plus Shadowing Reference Channel Model

Summing up, the reference model typically considered in the RSS-based ranging literature is the so-called *path-loss plus shadowing* model (or path-loss plus lognormal fading), according to which the *mean* received power at distance d from the transmitter can be expressed (in dBm) as

$$\bar{\mathcal{P}}_{\mathrm{rx}}(d) = D(d) + \Psi = \mathcal{K} - 10\eta \log\left(\frac{d}{\delta_0}\right) + \Psi, \tag{6}$$

where Ψ is a zero-mean Gaussian random variable with standard deviation σ_Ψ. This model provides the baseline for our analysis. Note that, for a given distance d, the time-averaged

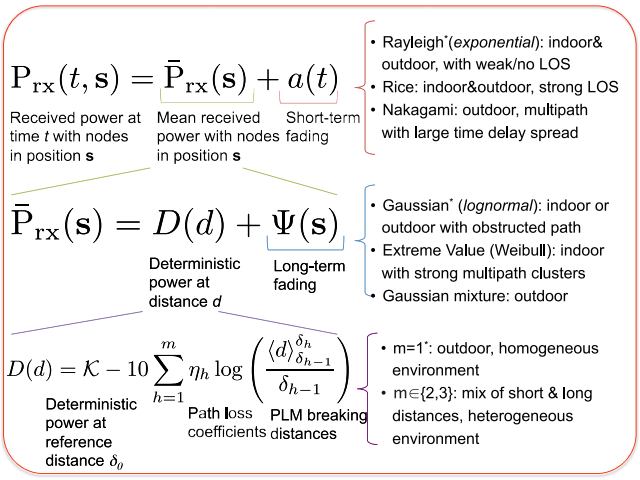

Fig. 1. Path loss models summary picture.

received power $\bar{\mathcal{P}}_{\mathrm{rx}}(d)$ is still stochastic, because of the shadowing term Ψ. The PDF of $\bar{\mathcal{P}}_{\mathrm{rx}}(d)$, hence, is a shifted version of the PDF of Ψ, i.e.,

$$f_{\bar{\mathcal{P}}_{\mathrm{rx}}(d)}(\mathrm{P_{obs}}) = f_{\Psi}(\mathrm{P_{obs}} - D(d)). \tag{7}$$

Fig. 1 offers a visual summary of the most popular PLMs considered in the literature, and of the statistical models used to describe their components (some of which will be discussed later on in the paper).

D. Reference RSS-Based Ranging Model

As mentioned, the RSS-based ranging consists in estimating the distance d between transmitter and receiver from the average signal power measured at the receiver. We recall that the average received power $\bar{\mathcal{P}}_{\mathrm{rx}}(d)$, as given in (6), is a random variable because of the fading term Ψ. Therefore, given an observation $\mathrm{P_{obs}}$ of $\bar{\mathcal{P}}_{\mathrm{rx}}$, the Maximum Likelihood Estimate (MLE) of the distance between the nodes is given by the value of d that maximizes the probability that $\bar{\mathcal{P}}_{\mathrm{rx}}(d) = \mathrm{P_{obs}}$, i.e.,

$$\begin{aligned}\hat{d}(\mathrm{P_{obs}}) &= \arg\max_{d\geq 0} f_{\bar{\mathcal{P}}_{\mathrm{rx}}(d)}(\mathrm{P_{obs}}),\\ &= \arg\max_{d\geq 0} f_{\Psi}(\mathrm{P_{obs}} - D(d)),\\ &= D_{\mathrm{inv}}(\mathrm{P_{obs}} - \mu_{\Psi});\end{aligned} \tag{8}$$

where the second step follows from (7), while in the last step we used $D_{\mathrm{inv}}(\cdot)$ to denote the inverse function of $D(\cdot)$, and μ_{Ψ} to indicate the mode that maximizes $f_{\Psi}(\cdot)$.

Observe that, when μ_{Ψ} depends on d, the computation of (8) may require numerical and iterative methods. Conversely, if μ_{Ψ} is invariant in d, then the distance estimate can be obtained with simple operations.

The accuracy of the estimation (8) depends on $D(\cdot)$ and on the statistical distribution of Ψ. Considering the reference model (6), the deterministic component is given by $D(d) = K - 10\eta\log(d/\delta_0)$, whose inverse is

$$D_{\mathrm{inv}}(x) = \delta_0 10^{(K-x)/(10\eta)}, \tag{9}$$

while the random term Ψ is modeled as a zero-mean normal random variable and, hence, its PDF is maximized at $\mu_{\Psi} = 0$. The distance estimate for a mean received power value $\mathrm{P_{obs}}$ is thus given by

$$\hat{d}(\mathrm{P_{obs}}) = D_{\mathrm{inv}}(\mathrm{P_{obs}}) = \delta_0 10^{\frac{\mathcal{K}-\mathrm{P_{obs}}}{10\eta}}, \tag{10}$$

which is likely the most widely used formula for RSS-based ranging.

Note that the estimate given by (10) is a deterministic function of the observed power $\mathrm{P_{obs}}$. However, for a given distance d, the received power may change because of the shadowing term, as for (6) and (7). Consequently, for a given distance d, the estimate $\hat{d}$ may change, depending on the actual position of the transmitter/receiver pair. To get a statistical characterization of $\hat{d}$ for a given distance d, we can replace $\mathrm{P_{obs}}$ in (10) with the random variable $\bar{\mathcal{P}}_{\mathrm{rx}}$, whose expression is given in (6), obtaining the following stochastic model for the distance estimate:

$$\hat{d}_{\mathrm{rnd}} = \delta_0 10^{\frac{10\eta\log(d/\delta_0)-\Psi}{10\eta}} = d\,10^{-\frac{\Psi}{10\eta}} = d\Psi_{\mathrm{LN}}^{-1/\eta}, \tag{11}$$

where we recall that Ψ_{LN} is the equivalent of Ψ in linear scale. The statistical distributions of Ψ and Ψ_{LN} are discussed in the Appendix.

E. Ranging Error Statistics

The *ranging error* can then be defined as the difference between the actual distance d and its estimate $\hat{d}$, i.e.,

$$\varepsilon(d) = d - \hat{d}. \tag{12}$$

Normalizing ε over the distance d we obtained the *relative ranging error*

$$\varepsilon_r(d) = \frac{\varepsilon(d)}{d}. \tag{13}$$

Using $\hat{d}_{\mathrm{rnd}}$ in place of $\hat{d}$ in the ranging error expressions, we can obtain the stochastic models for the absolute and relative ranging errors and, in turn, their mean and variance as functions of the real distance d and of the parameters of the channel model. From (12) we thus have

$$\varepsilon_{\mathrm{rnd}}(d) = d - \hat{d}_{\mathrm{md}} = d\left(1 - \Psi_{\mathrm{LN}}^{-1/\eta}\right), \tag{14}$$

and, under the customary assumption that Ψ_{LN} is lognormal distributed, we can express the statistical mean and variance of the ranging error as (see [20], [33]):

$$\mathrm{m}_{\varepsilon}(d) = d\left(1 - e^{\frac{\sigma^2}{2\eta^2}}\right); \quad \sigma_{\varepsilon}^2(d) = d^2\left(e^{\frac{\sigma^2}{\eta^2}} - 1\right)e^{\frac{\sigma^2}{\eta^2}}. \tag{15}$$

The mean and variance of the relative ranging error, instead, are equal to

$$\begin{aligned}\mathrm{m}_{\varepsilon_r}(d) &= \frac{\mathrm{m}_{\varepsilon}(d)}{d} = 1 - e^{\frac{\sigma^2}{2\eta^2}};\\ \sigma_{\varepsilon_r}^2(d) &= \frac{\sigma_{\varepsilon}^2(d)}{d^2} = \left(e^{\frac{\sigma^2}{\eta^2}} - 1\right)e^{\frac{\sigma^2}{\eta^2}}.\end{aligned} \tag{16}$$

From (15) and (16) it is apparent that the mean ranging error is negative, which means that the RSS-based ranging is, on average, affected by a positive bias, i.e., the estimated

distance is usually larger than the actual distance. Furthermore, both the bias and the variance of the estimate error worsen for higher values of σ, and larger distances. By knowing the value of σ, however, it is possible to remove the bias and reduce the estimate variance by dividing $\hat{d}$ over $\exp(\sigma^2/2)$, as proposed in [83]. Therefore, an accurate estimation of the variance of the shadowing term can greatly improved the accuracy of the RSS-based ranging.

F. Reference RSS-Based Ranging Procedure

The *naive* RSS-based ranging procedure is based on two assumptions:

i) RSS measurements can be uniquely mapped into the exact received signal powers (in dBm scale);

ii) the received signal power decreases with the distance d from the transmitter according to a deterministic and monotonic law.

Unfortunately, both these assumptions fail to apply in practice. In fact, the power-to-RSS transduction law is not always linear or exactly known, while the received power is typically affected by random noise terms due to signal propagation phenomena. These factors affect the accuracy of the RSS-based ranging to different extent, as will be discussed later on.

Accounting for these aspects, a proper method to exploit the RSS measurements for ranging purposes shall consists in the following steps.

1) **Calibration of raw RSS measurements:** mapping raw RSS measurements $\rho(t, \mathbf{s})$ into fairly accurate estimate of the received power $\mathrm{P}_{\mathrm{rx}}(t, \mathbf{s})$, by inverting (1).
2) **Time averaging:** reduction of the short-term fading component to get $\bar{\mathrm{P}}_{\mathrm{rx}}(\mathbf{s})$ as for (5).
3) **Path-loss model estimation:** estimation of the parameters $\mathcal{K}$, m, $\{\delta_h, \eta_h\}$, $h = 0, \ldots, m$ of the PLM (4).
4) **Analysis of the residual variability of the RSS measurements:** estimation of the statistical distribution of the long-term fading Ψ, considering all the collateral phenomena that may apparently increase its variance.
5) **RSS-based ranging:** mapping of the refined RSS measurements into a distance estimate by using (8).

The accuracy of the ranging estimate obtained by following this procedure, however, may be largely affected by the way these steps are implemented. In the rest of the paper, we analyze each step in greater detail, and investigate its potential influence on the accuracy of the RSS-based ranging.

Before delving into the topic, however, we present the experimental setup that have been used to back up the theoretical argumentation with empirical results.

V. Experimental Setup

To substantiate the argumentation developed in the next sections, we collected a number of RSS measurements by using some nodes of a testbed [84]–[87]. We first describe the hardware used in the experiments and, then, the different setups used to harvest RSS measurements.

We remark that the experimental measurements are unavoidably affected by the specificities of the technology used to collect the RSS measurements and, hence, the reported results have necessarily a local significance in their absolute values. Nonetheless, the lesson that can be learned from the trends observed in the reported results are rather general and apply to a much wider set of scenarios.

A. Hardware

All the experiments have been performed by using TmoteSky sensor nodes [88]. These devices are equipped with the Chipcon wireless transceiver CC2420, which is a very popular IEEE 802.15.4 radio used by Ember, MicaZ, Telos, Intel Mote2 and others. It operates in the 2.4 GHz ISM band using O-QPSK modulation with *Direct Sequence Spread Spectrum* (DSSS) coding. The radio module supports a maximum bitrate of 250 kbit/s, with -94 dBm of sensitivity, and provides two measurements related to the received signal quality, namely Radio Signal Strength (RSS) and Link Quality Indicator (LQI). In accordance with the IEEE 802.15.4 standard, the RSS value is averaged over 8 symbol periods (128 μs) [89]. A more detailed analysis of the functional aspects of the CC2420 transceiver and its RSS measurement circuit can be found in [35].

The transceiver makes use of a patch antenna, integrated on the board. As discussed in Section IX-A, the integrated antenna is not isotropic. However, the board is also equipped with an SMA connector for an external antenna that can be activated in place of the patch antenna by changing the electrical contacts of a capacitor. We made this hardware modification to a certain number of boards that were then equipped with a DN-70100 omnidirectional external antenna, produced by Digitus. The external antenna is 19.7 cm long, with a diameter of 12 mm, and provides a gain of 5 dBi (reception).

A simple communication protocol has been designed and developed in order to collect RSS samples over the 16 IEEE 802.15.4 RF-channels within the available $\mathcal{B} = 80$ MHz of the ISM band at 2.4 GHz.

B. Experimental Scenarios

We collected RSS data in six different scenarios, which have been specifically designed to gain insights on the different aspects that affect the accuracy of the RSS-based ranging. The scenarios are described below.

1) Antenna: This setup has been conceived to collect RSS samples at different distances d, and on different positions $\mathbf{s}$ for any given distance, thus making it possible to average out both the time-dependent and position-dependent fading terms. Furthermore, the scenario makes it possible to gain insights on the radiation pattern of the internal and external antennas.

The scenario consists of two nodes, A and B, which were placed at 30 cm from the floor of a wide empty room. Node A was kept fixed, while B was moved around A describing a circular trajectory of radius d, with angular steps of 10 degrees. The procedure was repeated varying the radius of the circular trajectory from 0.2 m to 2.4 m, with a step of 0.1 m. In each position, the nodes exchanged 10 packets either way, registering the RSS of each received packet, for a total of approximately 8280 RSS readings per node.

The experiment was repeated with three different configurations of node A, named `rotating` (`r`), `fixed` (`f`), and `external` (`e`). In the `rotating` mode, node A was equipped with the internal antenna and consistently rotated around its axis with B, in such a way that the relative orientation of the two devices and, in turn, their antenna gains, remained unchanged during the entire experiment. In the `fixed` case, instead, node A remained fixed in the original position, so that it faced node B from different angles as B rotated around it. The same setting was used for the `external` case, with the difference that node A was equipped with the external omnidirectional antenna, rather than the internal antenna, as in the other cases. In all the experiments, node B was rotated around its axis with a step of 10 degrees, while describing the circular trajectory, in order to always face node A with the same side. In this way, node B antenna gain in the LOS direction to A is constant.

2) Room: This scenario was conceived to collect RSS value at different distances, and over different carrier frequencies.

The scenario consists of four nodes, each equipped with the external isotropic antenna to avoid any issue related to antenna gains. Nodes were placed on cones at 30 cm from the floor, and programmed to exchange 20 packets with any other node, over a given RF channel. Consecutive transmissions from the same node were separated by at least 100 ms. The operation was repeated on all 16 RF channels, while keeping the nodes in the same positions. The whole process was repeated for 6 different locations of the nodes. Overall we collected $20 \times 12 \times 16 \times 6 = 23040$ RSS samples.

3) Desk: This scenario was conceived to assess the impact of different transmit powers and table surface reflections.

To this end, we placed two nodes, A and B, on a long desk. Both nodes were equipped with integrated antenna. Node A was fixed, while B was moved away from A along a straight line, while maintaining the same orientation to A. The distance between the nodes was increased from 0.2 m up to 7.2 m, with a step of 0.2 m. The transmit power of the nodes, instead, was varied in the set $\{0, -1, -3, -5, -7, -10 - 15, -25\}$ dBm, while the carrier frequency was changed over all the 16 available channels. For any combination of distance, transmit power, and RF channels, nodes exchanged 8 packets either way, for a total of 7378 RSS samples.

4) Aisle: This scenario was conceived to assess the performance of the RSS-based ranging in an aisle.

We deployed five sensor nodes on the top of 30 cm tall cones, resting on the floor along an aisle, and another sensor node was used to collect RSS samples at 26 locations spaced apart by 50 cm along a piece-wise linear path of approximately 13 meters that crossed the aisle. All nodes were equipped with external antennas. We collected both fixed-to-fixed and mobile-to-fixed two-way RSS measurements over all the 16 RF channels supported by the transceivers, for a total of approximately 4800 samples. In this environment there was no furniture so that the reflections of the transmitted signal were mainly due to the floor, the walls and the ceiling.

5) Lab: With a similar setting as AISLE, we deployed seven sensor nodes on cones in a lab of approximately 10×6 m^2. A further node was placed in different positions during the experiments. All nodes were equipped with external antennas. We collected both fixed-to-fixed and mobile-to-fixed two-ways RSS measurements over all the 16 RF channels, for a total of approximately 11000 samples. This environment was occupied by furnitures, electronic equipments, and people.

6) Outdoor: Five nodes were uniformly deployed over a 15×8 m^2 outdoor area, at 80 cm from the floor. Another node was moved through the area. All nodes were equipped with external antenna. We collected approximately 4800 RSS samples over 16 different RF channels.

In all the experiments we can assume LOS between each pair of nodes. Moreover, nodes were deployed at the same height, so that we cover only the case of 2–dimensional network deployment.[3]

In addition to these datasets, we also used some other measurements taken from public databases to investigate other scenarios, such as outdoor, non line-of-sight (NLOS), and so on. The references to such additional data sources are provided in Section XI where these other scenarios are discussed.

VI. Calibration of Raw RSS Measurements

In principle, the RSS value returned by the board (once converted and scaled as indicated by the data-sheet of the radio transceiver) should be equal to the received power in dBm scale, P_{obs}. In practice, the two values may differ for the following reasons:

(i) the RSS register can only take a finite number of values, so that it returns a *quantized* version of the actual received power, introducing a certain quantization error;
(ii) the transduction law may be irregular, e.g., piece-wise linear and even non-injective, in some intervals of the operating range;
(iii) the RSS readings of different nodes may be affected by different offsets.

These non-idealities generally have different effects on the RSS ranging accuracy, also depending on the specificities of the hardware. To substantiate our argumentation, we consider the characteristics of the CC2420 transceivers, produced by Texas Instruments [89], which is largely used in today platforms for WSNs.

A. RSS Granularity

According to the specification of the CC2420 transceiver, the RSS reading has a dynamic range of about 100 dB with a granularity of $\Delta_q \simeq 1$ dB. Therefore, assuming that the quantization error is uniformly distributed in the quantization interval, its standard deviation is approximately equal to $\sqrt{\frac{\Delta_q^2}{12}} \simeq 0.3$ dB, which is rather low and almost negligible in all practical cases. These considerations are confirmed by the experimental study presented in [35]. Similar values are also reported in the datasheets of other common radio transceivers. For example, the datasheet of the Low-Power Sub-1 GHz RF Transceiver CC1101 [90], produced by Texas

[3]The collected data can be downloaded from the SIGNET group website at http://telecom.dei.unipd.it/download or contacting the author.

Instruments, reports an RSS granularity of 0.5 dB, which is hence negligible.

B. RSS Non-Linearities

Let $\mathcal{R}_\circ(\cdot)$ represent the *nominal* power-to-RSS transduction law that characterizes the RSS circuit. Neglecting the quantization error, an ideal RSS circuit should implement a transparent transduction law, i.e., it should hold $\mathcal{R}_\circ(\mathrm{P_{obs}}) = \mathrm{P_{obs}}$ for all received power values in the operating range. Unfortunately, the RSS circuits do not generally provide such an ideal mapping. For instance, the transduction law provided by the CC2420 RSS circuit is shown in Fig. 2 by the black solid line with white circle markers, labelled as *raw RSS*. This curve reproduces the power-to-RSS curve reported by the manufacturer in [89, p. 48]. We can assume that the transduction law is deterministic, though small variations due to the operating temperature of the chipset or other non-idealities are possible. We note that the curve does not perfectly overlap with the diagonal dashed line that represents the ideal transduction law. Instead, $\mathcal{R}_\circ(x)$ is only piece-wise linear, and it is even non-injective in some intervals.

In this paper, we use the term *calibration* to indicate the operations that are intended to "rectify" the power-to-RSS transduction function, thus making it possible to unambiguously invert the $\mathcal{R}_\circ(x)$ function in order to obtain an estimate of x.

The $\mathcal{R}_\circ(x)$ function can be easily and unambiguously inverted in the injective regions. However, each RSS value that falls in a non-injective region can be associated to three distinct received power values. A possible technique to resolve this ambiguity consists in taking a combination of the uncertain values. For instance, let x_a, x_b, x_c be three power values that return the same RSS value ρ, i.e., such that $\mathcal{R}_\circ(x_i) = \rho$, $i = a, b, c$. We consider the following three possible RSS-calibration strategies to solve the uncertainty:

$$\texttt{Calibrate RSS (min)}\colon\ \mathcal{R}_\circ^{-1}(\rho) = \min\{x_a, x_b, x_c\},$$
$$\texttt{Calibrate RSS (mean)}\colon\ \mathcal{R}_\circ^{-1}(\rho) = (x_a + x_b + x_c)/3,$$
$$\texttt{Calibrate RSS (max)}\colon\ \mathcal{R}_\circ^{-1}(\rho) = \max\{x_a, x_b, x_c\}.$$

As an example, we consider the case of the CC2420 transceiver. The calibrated curves obtained with each of the three techniques are shown in Fig. 2, marked with triangles, asterisks, and squares, respectively. As we can see, the `Calibrate RSS (mean)` is quite close to the ideal curve (dashed line), though it still exhibits a deviation of ± 2 dB with respect to the actual received power $\mathrm{P_{obs}}$ in the first non-injective region, i.e., for $\mathrm{P_{obs}} \in [-60, -53]$ dBm, and ± 4 dB of deviation for $\mathrm{P_{obs}} \in [-30, -24]$ dBm.

A more sophisticated method to obtain unambiguous reverse mapping, suggested in [91], consists in performing multiple RSS measurements between the same pair of nodes by varying the transmit power, in the attempt of getting some RSS samples outside the non-injective regions.

Fig. 3 offers another example of a real RSS transduction law, as determined by the manufacturer of the chipset CC1101 for two different data rates at 868 MHz (see [90, p. 46]). We can observe that, also in this case, the transduction law is not perfectly linear, with an error with respect to the ideal line ranging from about -4.0 dB to 3.3 dB, excluding the saturation effects at the range boundaries. Furthermore, we observe that the transduction law changes with the transmit rate, which adds another element of variability.

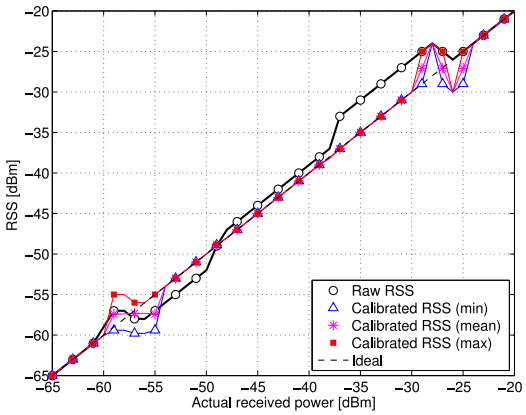

Fig. 2. RSS transduction law for CC2420 transceiver.

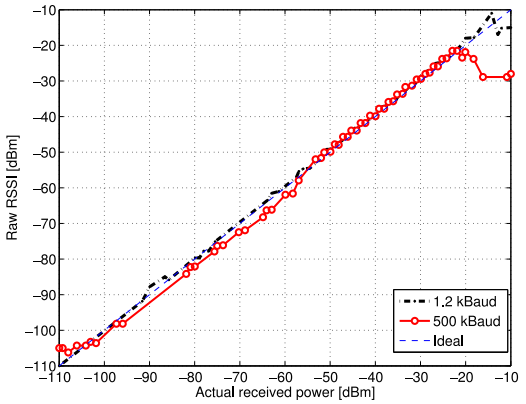

Fig. 3. RSS transduction law for the CC1101 transceiver at 868 MHz, at different transmit rates [90, p. 46].

These non-linearity of the RSS-to-power transduction laws can significantly affect the computation of the signal to noise power ratio (SNR) at the receiver, as experimentally observed in [91]. Also the estimate of the channel parameters obtained from the RSS measurements may be negatively affected by these singularities. A very basic and quite conservative strategy to avoid this problem is simply to neglect the RSS values in the non-injective regions when performing RSS-based ranging.

C. RSS Offset

The RSS measurements of different nodes may be affected by different offsets. For example, the CC2420 datasheet reports a tolerance of ± 6 dB for the RSS measurements, which may yield large uncertainty in the RSS ranging. The presence of such an offset can actually be experimentally observed with the platform used in our testbed. To this end, we consider the RSS measurements collected in the ANTENNA (e) and (r) scenarios, where we have constant antenna gains. To smooth out the effect of the short-term and long-term fading, we average all the RSS samples collected by each node at any given

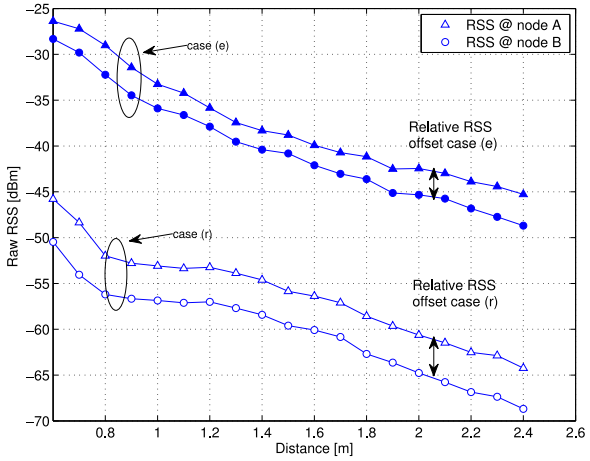

Fig. 4. Raw RSS *vs* distance in ANTENNA scenario, in the cases (e) and (r) (filled and empty markers, respectively).

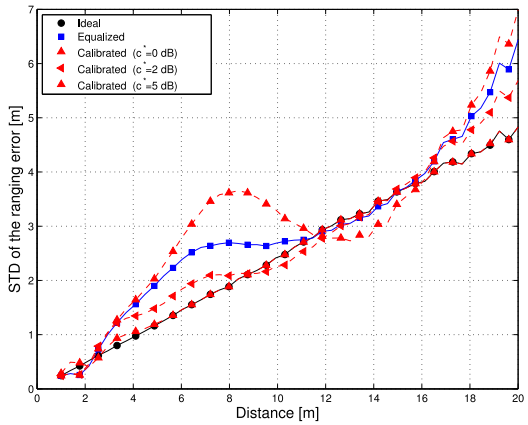

Fig. 5. Standard deviation of the ranging error, σ_ε, with $\mathcal{K} = -20$ dBm, $\delta_0 = 1$ m, $\eta = 2$, $\sigma_\Psi = 2$ dB, in the presence of non-ideal power-to-RSS mapping.

distance d. The resulting average RSS values are plotted in Fig. 4 for node A (Δ) and B ($\circ$).

At a first sight, we can see that the average RSS decreases almost linearly with the distance, in good agreement with the behavior predicted by the one-slope path-loss model (3). Second, we see that the RSS measured by nodes A and B are divided by a relative RSS offset of approximately 2.8 dB in the case (e) and 3.5 dB in the case (r).[4] Finally, we can note that the gap between the mean RSS curves for the two nodes is rather independent of the distance.

The experimental data confirm that the RSS offset of these devices is indeed additive and constant over the range of received power values. Therefore, the power-to-RSS map for a certain node j can be generally written as

$$\rho_j = \mathcal{R}_j(\mathrm{P}_{\mathrm{rx}}(t,\mathbf{s})) = \mathcal{R}_\circ(\mathrm{P}_{\mathrm{rx}}(t,\mathbf{s})) + c_j \qquad (17)$$

where c_j represents the RSS offset at receiver j.

Assuming symmetric propagation conditions, a rough estimate of the *relative* RSS offset between two nodes, i and j, can be obtained by exchanging multiple packets between the nodes and computing the difference between the mean RSS measured by each of them. If the RSS offset of node j is pre-compensated ($c_j = 0$), then this technique can be used to estimate and compensate the offset of the surrounding nodes, in a distributed manner.

Alternatively, it is possible to make all the nodes agree upon a common offset $c^\star$ by means of consensus techniques (see, e.g., [92]). In this case, the RSS reported by each node will be affected by the same constant offset $c^\star$, which will be eventually absorbed by $\mathcal{K}$ in (6). If $\mathcal{R}_\circ(x)$ is perfectly linear, this offset becomes totally irrelevant for RSS ranging, since it simplifies out when computing the distance estimate using (10). However, if the transduction law is only piecewise linear (as for the CC2420 transceiver), any offset, even common to all the nodes, may still significantly increase the variance of the ranging error.

[4]The relative RSS offsets in the cases (e) and (r) are different because we used two different devices as node A, one equipped with the external antenna and the other using the internal antenna. This also justifies the 20 dB gap between the RSS values collected in the cases (e) and (r).

To gain insights on the effect of non-linearities and offsets in the power-to-RSS transduction function, we generated 6000 synthetic realizations of received power values, according to the reference model (6) with parameters $\mathcal{K} = -20$ dB, $\delta_0 = 1$ m, $\eta = 2$, $\sigma_\Psi^2 = 2$ dB, for 50 different distances, uniformly distributed from 1 to 20 meters. Then, we mapped each received power value $\mathrm{P}_{\mathrm{rx}}(t,\mathbf{s})$ in a RSS value by using (17), where we used the CC2420 power-to-RSS function shown in Fig. 2 for $\mathcal{R}_\circ(\cdot)$. The values of RSS obtained in this way were then used to perform RSS-based ranging estimates.

Fig. 5 plots the standard deviation $\sigma_\varepsilon(d)$ of the ranging error we obtained when varying the transmitter-receiver distance d. The different curves correspond to different ways to map the RSS values back into an estimated receive power value $\mathrm{P}_{\mathrm{obs}}$, which is then used in the ranging equation (10). We considered the following cases.

Ideal: It assumes perfect power-to-RSS mapping and zero offset, i.e., $\mathrm{P}_{\mathrm{obs}} = \mathcal{R}_\circ(\mathrm{P}_{\mathrm{rx}}(t,\mathbf{s})) = \mathrm{P}_{\mathrm{rx}}(t,\mathbf{s})$. It is used as benchmark to evaluate the impact of the non idealities in the power-to-RSS mapping.

Equalized: It assumes the same RSS offsets $c^\star$ for all nodes, but no further calibration of RSS measurements is considered. In other words, the transduction function is given by $\mathrm{P}_{\mathrm{obs}} = \mathcal{R}_\circ(\mathrm{P}_{\mathrm{rx}}(t,\mathbf{s})) + c^\star$. We remark that, in this case, $c^\star$ simplifies out in (10), therefore the ranging accuracy is only affected by the non-linearities of the $\mathcal{R}_\circ(\cdot)$ function.

Calibrated: It considers the calibration of the raw RSS values by inversion of $\mathcal{R}_\circ(\cdot)$ using the "mean" criterion in the non-injective regions, but without compensation for the RSS offset. Hence, it gives $\mathrm{P}_{\mathrm{obs}} = \mathcal{R}_\circ^{-1}(\mathcal{R}_\circ(\mathrm{P}_{\mathrm{rx}}(t,\mathbf{s})) + c^\star)$.

Comparing the curves, we can see that the RSS calibration actually brings some improvement over the offset equalization only when the RSS offset is less than few dBs. Instead, performing the RSS calibration in the presence of non-negligible offsets may significantly worsen the ranging error.

This leads to the conclusion that, when the power-to-RSS transduction law is not perfectly linear, *the RSS calibration shall be considered only when the RSS offsets can be accurately estimated and compensated for.* Otherwise, it is more effective to elect a reference node and equalize the

RSS readings with respect to a common (though unknown) RSS offset $c^\star$, without trying to correct the non linearities of $\mathcal{R}_\circ(\cdot)$.

VII. Time Averaging

Once refined the RSS measurements, the next operation which is typically performed to improve the accuracy of the RSS-based range estimate is to average out the fast fading term $a(t)$ to get $\bar{\mathrm{P}}_{\mathrm{rx}}(\mathbf{s})$ (see (2) and (5)). This operation, though trivial, still requires some care. In fact, it can be performed either in the linear or logarithmic scale, with different results, as it will be discussed in the following.

A. Fast Fading Models

We start by recalling some common statistical models for the fast fading term, referring to the Appendix for the mathematical details. A well-accepted model is the so-called *Rician fading*, according to which the fading coefficient in linear scale, $a_{\mathrm{LN}}(t)$, is modeled as the module of a complex Gaussian process, which is distributed as a Rice random variable. The model is suited to describe the amplitude distribution of a received signal given by the overlapping of a Line-of-Sight component and a number of scattered replicas. The Rice distribution is indeed characterized by two parameters: the so-called *Rice Factor*, R_F, which is given by the ratio between the power in the direct path and the power in the other, scattered, paths; and the overall signal power [82]. Larger values of R_F indicates the dominance of the LOS path over the reflected paths, so that the amplitude of the received signal becomes less erratic. Accordingly, the variance of $a_{\mathrm{LN}}(t)$, derived in the Appendix, decreases approximately as $1/R_F$ as R_F grows.

Another common model for the short-term fading is the *Rayleigh fading* model, which is suitable in the presence of several multipath components without dominant LOS ray, and can be obtained from the Rice model by setting $R_F = 0$. In this case, $a_{\mathrm{LN}}(t)$ is modeled as an exponential-distributed random variable, with unit mean and variance, whose simplicity and mathematical tractability have greatly contributed to the popularity of the Rayleigh model in the literature.[5]

B. Getting Rid of the Fast Fading Term

As mentioned, the time-varying random term $a(t)$ in (2) is usually disregarded, under the assumption that it can be smoothed out by averaging RSS samples taken over a suitable time window. However, the time average can be computed either in linear scale, and then converted back in dB scale, or directly in dB scale. We will denote by $\bar{a}(N)$ the average computed over N RSS values in linear scale and then converted in dB, and by $\overline{a(N)}$ the average of the N RSS values performed directly in dB scale. We observe that these averages are random variables, depending on the realization of the N considered RSS samples. To compare the two approaches, we can hence resort to the statistical mean and standard deviation of these averages, whose expressions are derived in the Appendix.

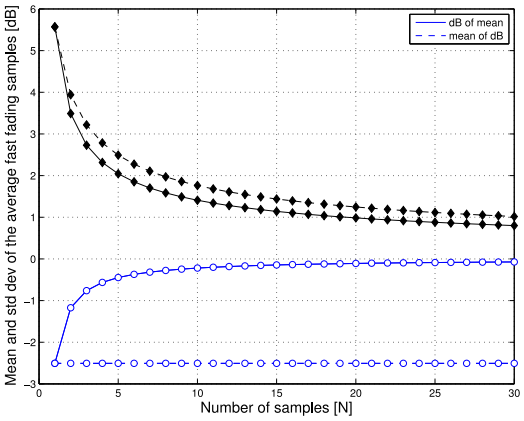

Fig. 6. Mean ($\circ$) and standard deviation ($\diamond$) of $\bar{a}(N)$ (solid lines) and $\overline{a(N)}$ (dashed lines) when varying the number of samples N.

A direct comparison of the statistics of $\bar{a}(N)$ and $\overline{a(N)}$ is given in Fig. 6, which reports mean and standard deviation of the two random variables when varying the number N of averaged samples.

At a first look, we note that $\bar{a}(N)$ exhibits lower standard deviation than $\overline{a(N)}$, though the difference is practically negligible. Furthermore, we note that the two standard deviation curves show an initial steep decrease, followed by a flatter behavior for larger values of N, so that decreasing the standard deviations below 1 dB requires a rather large number of samples, which means large energy costs and relatively long delays. For example, the coherence time of a Rayleigh fading channel at 2.4 GHz, with an equivalent relative speed between transmitter and receiver of 2 m/s, is approximately 80 ms. Therefore, collecting $N = 30$ fading samples, sufficiently spaced apart to be almost uncorrelated, would require at least $T = 2.4$ s. We also note that the average in dB scale exhibits a non-zero mean, i.e., a bias, which is not present in the other case.

In conclusion, it is slightly more convenient to average out the fast fading term in linear scale and, then, convert the result back in dB scale. Furthermore, increasing the number N of RSS samples beyond a few units, say 10 or 15, has diminishing effect in reducing the variance of the residual fading term.

VIII. Path-Loss Model Estimate

Once refined the RSS measurements and averaged out (as far as possible) the slow-term fading component, we are ready to estimate the parameters of the propagation model. This operation is sometimes referred to as *channel calibration* [93]–[95], though in this work we prefer to reserve the word "calibration" to the operations aimed at rectifying the power-to-RSS transduction function $\mathcal{R}(\cdot)$.

We then suppose to have collected a column vector $\mathbf{R} = [r_1, \ldots, r_M]^{\mathrm{T}}$ of time-averaged RSS values, measured over known distances $\mathbf{d} = [d_1, d_2, \ldots, d_M]^{\mathrm{T}}$. In practice, the vector $\mathbf{R}$ can be built by collecting RSS measurements between a certain number of anchor nodes. Otherwise, it is possible to

[5] Although there are many other statistical models to describe the fast fading component of a wireless signal (e.g., Nakagami, Weibull, Suzuki), we limit our attention here to the Rice and Rayleigh fading models because they are by far the most common in the literature dealing with RSS-based ranging.

perform a site survey with a certain number of probing nodes placed at different distances.

Neglecting the non-idealities of the power-to-RSS transduction law $\mathcal{R}(\cdot)$ (i.e., assuming perfect calibration), the average RSS samples can be expressed as in (5), i.e., for $i = 1, \ldots, M$ we can write

$$r_i = D(d_i) + \Psi = \mathcal{K} - \sum_{h=1}^{m} 10\eta_h \log\left(\frac{\langle d\rangle_{\delta_{h-1}}^{\delta_h}}{\delta_{h-1}}\right) + \Psi; \qquad (18)$$

where the right-most term follows from (4). The objective of the PLM parameters estimation is to find the values of $\mathcal{K}$, m, and $\{\delta_h, \eta_h\}$, with $h \in \{0, \ldots, m-1\}$, that best fit the empirical data, i.e., that minimize the mean squared error (MSE) between the observed RSS values and the expected RSS values given by (4) at the same distances.

The choice of the number of pieces of the path-loss model, m, is somehow arbitrary. A common approach is to plot the collected RSS measurements over the sampling distances in logscale and to visually determine the number of slopes of the piece-wise linear trajectory that best interpolate the points. We observe that the larger the number of breakpoints m, the larger the number of parameters of the PLM to be estimated and, hence, the higher the computational complexity and the lower the accuracy of such estimates for a given number of RSS samples. Moreover, the risk of overfitting also increases with m. As a practical rule, m should be fixed to the smallest value for which the RSS samples appear evenly distributed (in dB scale) around the piece-wise PLM for most of the distances, with approximately constant standard deviation. Furthermore, the resulting piece-wise linear characteristic should be convex and monotonic decreasing with the distance, since the attenuation is usually more pronounced for larger distances. In most practical cases, a good fitting of the RSS samples can be obtained with $m \leq 3$ (see [78]).

Similarly, the value of the breakpoints $\{\delta_h\}$ can be taken from the literature, depending on the specific environment where the RSS measurements are collected, or determined based on common sense, from direct "visual" inspection of the RSS measurements, or even selected by means of a brute-force semi-exhaustive search of all reasonable combinations of the parameters.

Given the breakpoints $\{\delta_h\}$, $h \in \{0, \ldots, m-1\}$, it is possible to estimate the other parameters of (4) by using, for instance, the least square method that minimizes the MSE between predicated and measured RSS values. More specifically, the MSE can be expressed as

$$\mathbf{MSE} = (\mathbf{R} - \mathbf{X}\,\mathbf{p})(\mathbf{R} - \mathbf{X}\,\mathbf{p})^{\mathrm{T}} \qquad (19)$$

where $\mathbf{p} = [\mathcal{K}, \eta_1, \ldots, \eta_m]^{\mathrm{T}}$ is the parameters vector, and

$$\mathbf{X} = \begin{bmatrix} 1 & -10\log\dfrac{\langle d_1\rangle_{\delta_0}^{\delta_1}}{\delta_0} & \cdots & -10\log\dfrac{\langle d_1\rangle_{\delta_{m-1}}^{\infty}}{\delta_{m-1}} \\ \vdots & & & \\ 1 & -10\log\dfrac{\langle d_M\rangle_{\delta_0}^{\delta_1}}{\delta_0} & \cdots & -10\log\dfrac{\langle d_M\rangle_{\delta_{m-1}}^{\infty}}{\delta_{m-1}} \end{bmatrix}. \qquad (20)$$

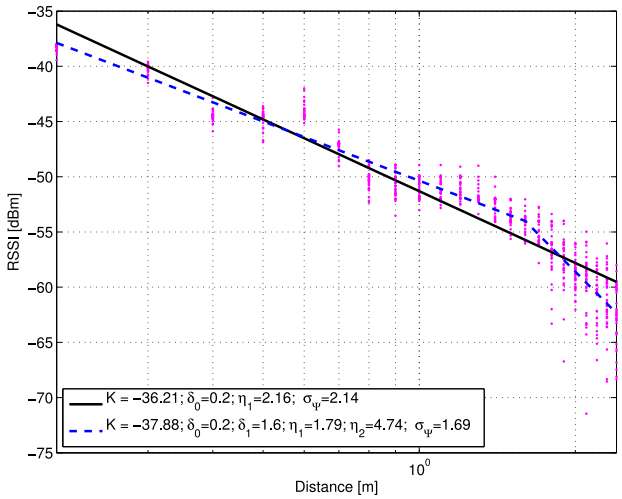

Fig. 7. Comparison between the channel parameters estimate obtained with one-slope (solid line) and two-slope (dashed line) PLM. Markers show the (time averaged) RSS values collected in the ANTENNA(r) scenario.

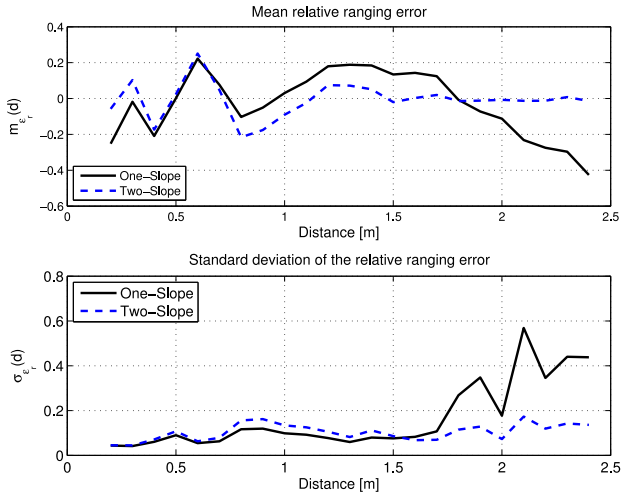

Fig. 8. Mean (upper plot) and standard deviation (lower plot) of the relative ranging error ε_r when varying the distance d in the ANTENNA(r) scenario, for the one-slope (solid lines) and two-slope (dashed lines) PLM.

Using the least square method, the vector $\hat{\mathbf{p}} = [\hat{\mathcal{K}}, \hat{\eta}_1, \ldots, \hat{\eta}_m]^{\mathrm{T}}$ of estimated parameters is then obtained as:

$$\hat{\mathbf{p}} = \left(\mathbf{X}^{\mathrm{T}}\mathbf{X}\right)^{-1}\mathbf{X}^{\mathrm{T}}\,\mathbf{R}. \qquad (21)$$

Note that, to reduce clutter, in the following we will use the same notation for actual and estimated parameters, unless an explicit distinction is required to avoid ambiguity.

A. Empirical Analysis of Path-Loss Model Estimate

To appreciate the effect of a multi-slope PLM, we applied (21) to the (time-averaged) RSS measurements collected by node A in the ANTENNA(r) scenario in two cases, namely with $m = 1$ (one-slope model), and $m = 2$ (two-slope model).

Fig. 7 shows the empirical RSS measurements (dots), together with the theoretical values returned by the one-slope model (solid line) and the two-slope model (dashed line),

whose parameters are reported in the figure's legend. We can observe that, in this particular case, the two-slope model is capable of better fitting the empirical data, thus reducing the MSE, i.e., the variance of the shadowing term[6] σ_Ψ^2. The better fitting of the two-slope model with empirical data is reflected by a reduction of the mean and the standard deviation of the relative ranging error (15), shown in the upper and lower graphs of Fig. 8. In particular we note that the relative ranging error obtained using the two-slope model is less sensitive to the distance, with a standard deviation that, for the considered case, always remains below 20%.

IX. Analysis of the Residual Variability of the RSS Measurements

From the estimate $\hat{\mathbf{p}}$ of the parameters of the PLM it is possible to compute $D(d_i)$ for any distance d_i, i.e., the deterministic component of (18). According to that model, the difference between expected and measured RSS values is ascribed to the long-term fading Ψ.

Indeed, according to (18), the vector of shadowing coefficients that affect the M averaged RSS values $\mathbf{R}$ can be expressed as

$$\hat{\Psi} = \mathbf{R} - \mathbf{X}\,\hat{\mathbf{p}}, \tag{22}$$

where we have used the vectorial representation introduced in the previous section. The mean and variance of Ψ can hence be estimated, respectively, as

$$\mathrm{m}_\Psi = \frac{\sum_{k=1}^{N} \hat{\Psi}_k}{N},\ \sigma_\Psi^2 = \frac{\sum_{k=1}^{N} \left(\hat{\Psi}_k - \mathrm{m}_\Psi\right)^2}{N-1}. \tag{23}$$

In this way, however, the statistical power of the long-term fading is inflated by external factors that are not connected with the fading process and, then, can worsen the accuracy of the RSS-based ranging. In fact, we observe that σ_Ψ^2, computed as in (23), actually absorbs the power of all residual noise sources, such as errors in the path-loss parameter estimates, non-idealities in the power-to-RSS transduction law, position-dependent variations of the channel parameters, and so on. Therefore, the value of σ_Ψ^2 estimated from (23) may result much larger than the actual variance of the shadow fading that characterizes the considered environment.

In the following of this section, we analyze some of the factors that may contribute to inflate the estimated power of this noise term. Then, we explain the *multichannel RSS averaging* technique, which has been proposed in [96] as an effective and simple strategy to reduce the space variability of the RSS measurements. Finally, we present empirical results that show the impact of different RSS-refinement techniques on the estimated variance of Ψ.

A. Technical Pitfall: Antenna Radiation Pattern

In many studies, the antenna orientation of the transceivers is random and the antenna radiation pattern is usually overlooked or implicitly assumed isotropic. Unfortunately, the antenna supplied with most low-end wireless devices may be somewhat anisotropic [97].

[6]Note that, in the figure, we reported σ_Ψ rather than σ_Ψ^2 to allow for a direct comparison of the error with the RSS values.

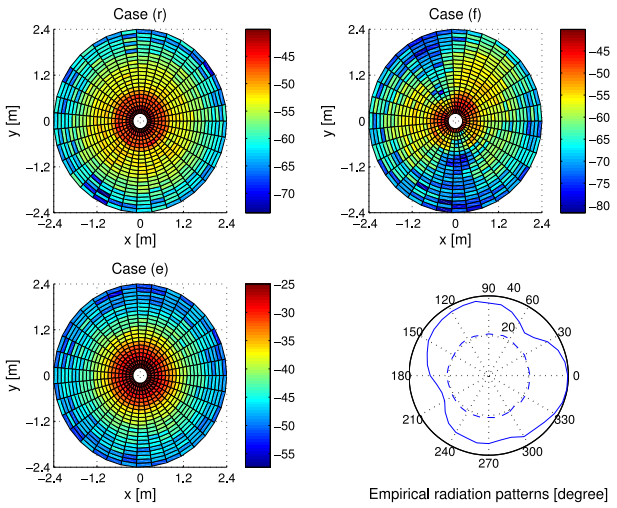

Fig. 9. Upper-left and right, and lower left: colormaps of the mean RSS in ANTENNA scenario, cases (r), (f), (e), respectively. Lower-right: empirical antenna radiation patters of the internal (solid) and external (dashed) antenna.

The resulting increase of RSS variability may be erroneously ascribed to the propagation conditions that, hence, would result harsher than they actually are, thus contributing to bring discredit on RSS for ranging purposes [98].

The ANTENNA scenario makes it possible to appreciate the effect of the anisotropic radiation pattern of the TmoteSky integrated antenna on the RSS reliability. The RSS samples collected in the experiments (r), (f) and (e) are plotted in Fig. 9, together with the empirical radiation pattern for the integrated and external antenna, suitably scaled for image clarity. The first three plots in the figure show the colormap of the time-averaged RSS values measured on the different positions: the darker the color, the lower the mean RSS value.

As expected, the RSS decreases when moving from the center to the periphery of the plot, i.e., increasing the distance between transmitter (node A) and receiver (node B). In case (r), the mutual antenna orientation between A and B is maintained fixed, so that the antenna gains do not change with the position of B. We observe that the RSS is roughly homogeneous in all directions, except for small variations likely due to shadowing phenomena. In case (f), instead, the orientation of the two antennas varies as B moves along the circular trajectory around A. Here the gain greatly changes with the direction as a consequence of the anisotropy of the integrated antenna. Finally, the rather homogeneous decrease of the measured RSS values observed in case (e) confirms the isotropic emission pattern of the external antenna.

These conclusions can be better appreciated from the antenna radiation patterns reported in the lower-right plot of Fig. 9, from which we can notice that the integrated antenna (solid line) is not isotropic in the horizontal plane, but instead, presents three main lobs, roughly spaced by an angle of $2\pi/3$. The difference between the maximal and minimal gain is about 15 dB. This empirical radiation pattern closely resembles that reported in the TmoteSky datasheet for

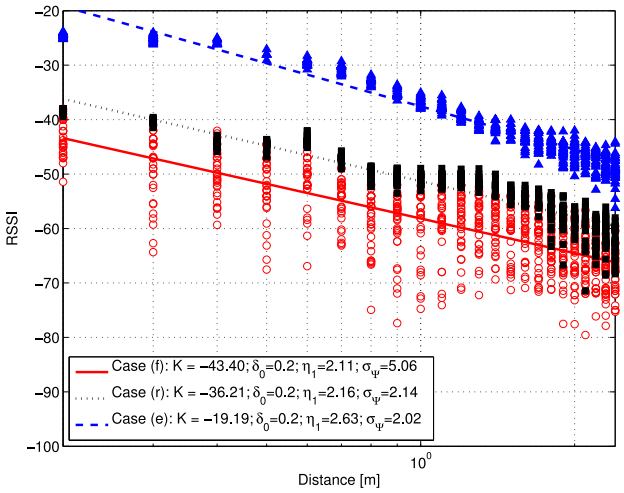

Fig. 10. Raw RSS values (markers) and one-slope path-loss curve (lines) in the ANTENNA scenario.

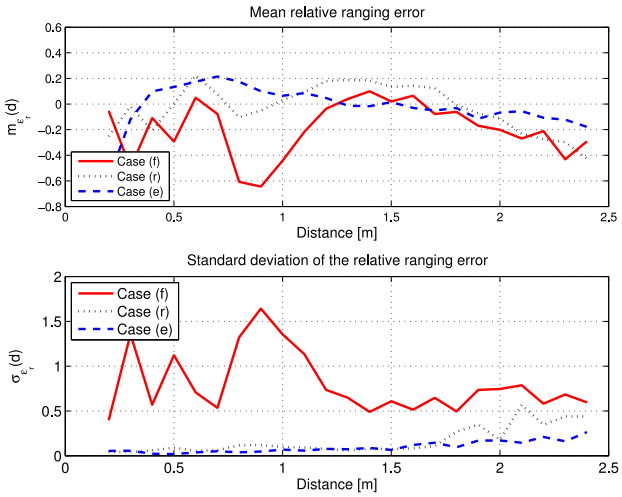

Fig. 11. Relative ranging error mean (upper plot) and standard deviation (lower plot) when varying the distance d, with raw RSS values, in the ANTENNA scenario.

the Inverted-F antenna with vertical mounting [88]. The radiation pattern obtained for the external antenna (dashed line) is much more regular, with a maximum peak difference of 1.4 dB only.

Although these results have been obtained with a specific technology, the problem of anisotropic radiating antennas is rather general. Other examples can be found, e.g., in [97], where it is reported that a specific Printed Circuit Board (PCB) antenna, suitable for very low-cost devices, have 5.16 dB higher radiated power in the direction of maximum emission compared to an ideal isotropic antenna, and -12.81 dB lower transmit power in another direction.

It is now interesting to analyze the effect of the antenna anisotropy on the channel parameters estimate. To this end, we report in Fig. 10 the RSS values collected by the nodes in cases (f), (r), and (e). Furthermore, we report the one-slope path-loss curves obtained in the three cases by using the least square method described in (21). The estimated channel parameters are reported in the legend of the figure.

We see that the estimate of $\mathcal{K}$ changes in the three cases due to the different mean antenna gains. What is more interesting is that the estimate of the path-loss coefficient η_1 is approximately the same (around $\eta_1 \simeq 2.2$) in all the cases, while the estimate of the shadowing standard deviation changes significantly, from 5.06 dB for case (f) to 2.14 dB and 2.02 dB for cases (r) and (e), respectively. This means that the antenna anisotropy, when neglected, may yield an overestimation of the shadowing variance of several dBs (about 3 dB in our study).

The effect of the antenna anisotropy in terms of ranging error is shown in Fig. 11. The upper and lower plots report the mean and standard deviation of the relative ranging error ε_r, defined in (13), when varying the distance d between the nodes. We observe that the RSS ranging error is significantly larger in case (f) than in the other two cases. In particular, the standard deviation of the ranging error in case (f) is always above 50% of the actual distance, whereas it is below 20% for most of the distances in the other cases, where the effect of the antenna anisotropy is avoided, though it tends to increase at larger distances.

In conclusion, the TmoteSky integrated antenna is not suitable for a reliable RSS measurement. The solution to this problem might be the use of external isotropic antennas. Also in this case, however, it shall be noted that the isotropy is typically guaranteed on the planar plane, i.e., when all the nodes are deployed at the same height [98]. Another option is to equalize the antenna anisotropy at the receiver, provided that the radiation patterns and the mutual orientation of the nodes are known.

B. Methodological Pitfall: Packet Reception Probability

A fact that is often overlooked when performing RSS-based ranging is that RSS measurements are typically taken only for correctly received packets. Actually, in many commercial transceivers the RSS value can be continuously read from a suitable register. However, the value is frozen when the demodulator detects a valid signal preamble and (usually) appended after the packet payload, thus becoming easily accessible to the upper layers (see, e.g., [90, p. 44]). In most of the RSS-based works, the RSS values are thus extracted from the received packets, rather than read from the RSS register. Therefore, if a signal is too weak to be decoded, its RSS is typically disregarded, so that the recorded RSS values always refer to signals received with power above the sensitivity level of the receiver. The statistical distribution of such RSS values is then conditional on the good reception of the packet and, hence, may offer a biased representation of the actual channel conditions. To account for this effect, the expression (18) of the measured RSS can be corrected as

$$r_j = D(d) + \mathring{\Psi}; \tag{24}$$

where $\mathring{\Psi}$ is the conditional shadowing term, given that the packet has been correctly received. Note that $f_{\mathring{\Psi}}(a)$ depends on the distance d: the closer the distance to the reception range,

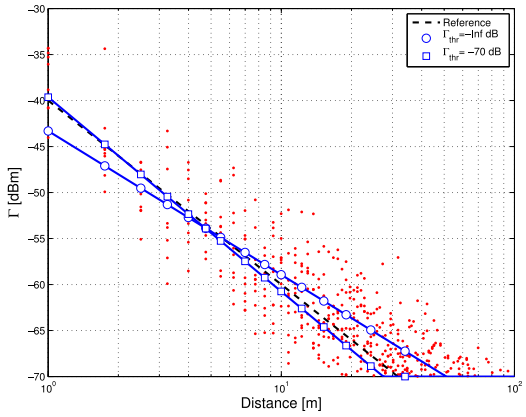

Fig. 12. Example of the impact of the power reception threshold on the estimation of the PLM parameters.

the more significant the bias of $\mathring{\Psi}$ with respect to the nominal distribution of Ψ. Neglecting this bias may worsen the accuracy of the channel parameters estimate, thus yielding a degradation of the RSS-based ranging accuracy. It is hence important to estimate the channel parameters by using only *unbiased* RSS measurements. The problem is to discriminate between unbiased and biased RSS values.

In the Appendix we propose a simple method to estimate the critical distance d° within which $\mathring{\Psi}$ has approximately the same distribution as Ψ, i.e., the RSS samples are likely unbiased. Considering only the RSS samples collected at distances less than d° we can then apply the least square parameters estimation method in its classical form (21).

This shrewdness is actually meaningful only when many measurements are collected at the edge of the reception range, and when the shadowing term exhibits large variance. An example of such a scenario is reported in Fig. 12, where we show a simulation of the simple path-loss plus shadowing channel model with parameters $\mathcal{K} = -20$ dB, $\delta_0 = 0.1$ m, $\eta_1 = 2$, $\sigma_\Psi = 4$ dB. The dashed line shows the actual deterministic path-loss component $D(d)$ given by (3) with these parameters. Dots represent the RSS samples, which have been generated at random distances, uniformly spaced in the range $[1, 150]$ meters. We assumed a reception sensitivity of $\Gamma_{\mathtt{thr}} = -70$ dBm, so that all RSS values below this reception threshold have been neglected and do not appear in the figure. Square/circle markers denote the PLMs obtained by considering/neglecting the power reception threshold in the estimation of the PLM parameters, respectively. We can see that the PLM obtained by considering the reception threshold $\Gamma_{\mathtt{thr}} = -70$ dBm is closer to the one used to generated the data (dashed line), while the PLM obtained by neglecting the effect of the receiver sensitivity (i.e., assuming $\Gamma_{\mathtt{thr}} = -\infty$ dBm), exhibits a significant bias that, in turn, yields worse ranging accuracy.

C. Multichannel RSS Averaging

As observed in [96], multichannel diversity has seldom been used in the context of RSS-based ranging as a simple and effective way to improve ranging accuracy. This neglectfulness is partially due to the common practice of ascribing the space-variability of the RSS measurements to the shadow fading, which models the random attenuation of signal power due to path obstruction. As a matter of fact, the spatial diversity brought in by carrier frequency shifts is basically ineffective to counteract this type of shadowing phenomena.

However, the space variability of the RSS measurements may also be the result of the combination of the proper shadow fading and the *strong self-interference* generated by a few strong reflections of the transmitted signal [78], [99], [100]. As shown in [96], indeed, a propagation environment characterized by a few clusters of reflected waves may yield a statistical distribution of the term Ψ closer to the Extreme Value than the normal distribution.[7] The Extreme Value distribution has also been empirically observed in many different experimental campaigns, both in indoor and outdoor environments [34], [101]–[103].

In this case, multichannel average can be effective, since it decreases the influence of the space-dependent fading component due to signal self-interference [96], [104], [105]. Furthermore, as shown in [96], the average of multiple RSS samples collected on different RF channels exhibits again a lognormal distribution, with a significant lower standard deviation than the original RSS samples.

The actual effectiveness of multichannel average, therefore, strongly depends on the characteristics of the propagation environment. If the delay spread of the channel is very small, i.e., all multipath components arrive at the receiver almost simultaneously, a change in the carrier frequency will be basically ineffective. Conversely, in the presence of a few clusters of waves, sufficiently spaced apart in time, the multichannel averaging may actually bring a significant reduction of the shadowing variance. For instance, the IEEE 802.15.4 specifications define 16 RF channels evenly distributed over $\mathcal{B} = 80$ MHz of the ISM band at 2.4 GHz. At these frequencies, the typical delay spreads τ in indoor environments range from tens to hundreds of nanoseconds [106], [107]. Therefore, the product $\mathcal{B}\tau$ is typically larger than one and, consequently, multichannel RSS averaging is expected to be rather beneficial.

It is worth remarking that the main advantage of multichannel RSS averaging is its simplicity. However, it does not fully exploit the information on the frequency component of the received signals, embedded in the multichannel RSS measurements. More effective approaches are described in [104] and [105].

D. Empirical Analysis of the Long-Term Fading Distribution

To appreciate the effect of the different RSS refinement techniques on the estimated variance of Ψ, we consider the RSS measurements collected in the ROOM scenario, where the relative RSS offsets $\{c_j\}$ of all nodes are known in advance and, hence, can be compensated to equalize the RSS readings. With this setup, we collected RSS samples at different time instants

[7] A brief description of these statistical models for the long-term fading is given in the Appendix.

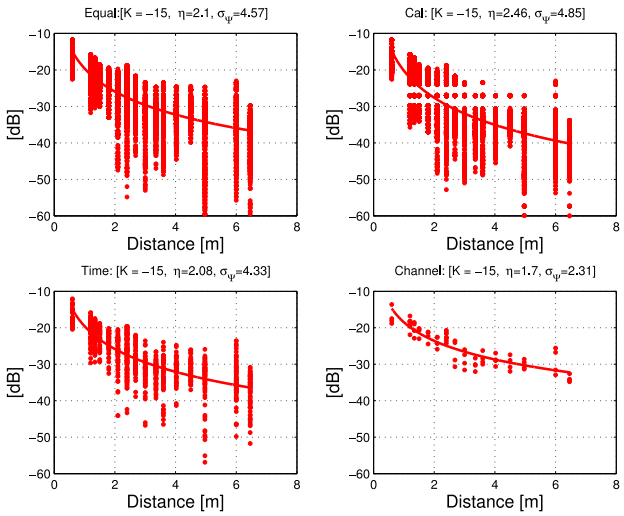

Fig. 13. RSS data and channel parameters estimate after successive refinement steps: offset compensation (upper-left), calibration (upper-right), time-average (lower-left), channel-average (lower-right). ROOM scenario.

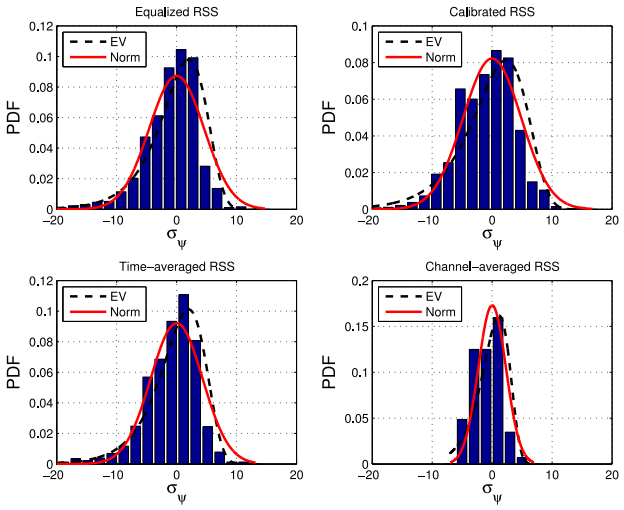

Fig. 14. Empirical PDF of the RSS error (bar), with Normal fit (solid) and Extreme Value fit (dashed). ROOM scenario.

and over all the 16 available RF channels supported by the CC2420 transceiver. This set of raw RSS measurements has then been processed through a cascade of refinement steps, namely:

`Equal`: offset equalization;
`Cal`: RSS calibration, i.e., inversion of $\mathcal{R}_\circ(\cdot)$;
`Time`: time averaging;
`Channel`: frequency averaging.

These refinement steps are applied in sequence so that, in the `Channel` case, the data are compensated for the RSS offsets, calibrated, time averaged, and frequency averaged. Averages are always performed in linear scale and the result converted back in dB scale. The four resulting datasets are then used to estimate the channel parameters and the standard deviation of the long-term fading by using (21) and (23), and considering a simple PLM with $m = 1$ and $\delta_0 = 0.6$ m.

The results are reported in the four graphs of Fig. 13. The refined RSS samples are represented by markers, while the estimated deterministic component $D(d)$ is reported in solid line. Comparing the figures and the values of the estimated channel parameters reported above each graph we can make some interesting observations.

First, we observe the peculiar distribution of the points in the interval $[-30, -25]$ dB, on the upper-right graph of Fig. 13, which is due to the reverse mapping of the $\mathcal{R}_\circ(x)$ curve in the non-injective regions using the "mean" criterion (see also Fig. 2). Comparing the upper-right and the lower-left graphs, we note that the time averaging has negligible effect on the estimate of σ_Ψ, which leads to the conclusion that, in this scenario, the short-term fading has limited impact on the RSS variability. This result is probably due to the presence of a dominant component in the received signal, compatible with a Rician fading model with very large Rice factor. Conversely, looking at the last graph, we note that the multichannel averaging yields a significant reduction of σ_Ψ, which drops from about 4.3 dB down to 2.3 dB. Very similar results have been observed in other scenarios, both indoor and outdoor, not reported here for the sake of conciseness.

From the rich data set collected in the ROOM scenario we could also derive a complete statistical characterization of the error term Ψ. Fig. 14 reports the empirical PDF of Ψ (blue bars), together with its Normal fit (solid line) and Extreme Value fit (dashed line), for each of the four data refinement steps discussed above. We can see that the empirical PDF of Ψ in the first three cases (equalized, calibrated, and time-averaged) is closer to the Extreme Value than the Normal distribution, whereas in the fourth case the normal distribution fits better. However, a more objective analysis of the empirical distribution of Ψ reveals that, in the first three cases, the null hypothesis for either the Extreme Value and the Normal distribution is rejected by the Kolmogorov-Smirnov (KS) goodness-of-fit hypothesis test. Instead, the Normal null hypothesis is accepted by the KS test in the last case. We can then conclude that, for the data set collected in the ROOM scenario, the error term Ψ obtained from equalized/calibrated/time-averaged RSS data exhibits a non-classical probability distribution (though more similar to the Extreme Value than the Normal), whereas the Normal distribution of Ψ (lognormal in linear scale), typically assumed in the papers dealing with RSS ranging, is actually verified only after the last refinement step, i.e., when the RSS samples are averaged over multiple RF channels.

All these results find a theoretical justification in a multi-cluster channel propagation model, as explained in [96]. Indeed, we have been able to replicate the empirical distribution of the RSS samples collected in the ROOM scenario by simulating a channel model consisting of $N = 6$ clusters, each characterized by a uniform random phase, and an amplitude with mixture distribution, inspired by the Suzuki fading model [108], which combines a Rice distribution with Rice factor $R = 20$, with a random statistical power, having log-normal distribution with parameters $\mu = 0$ and $\sigma = 2/\xi$.

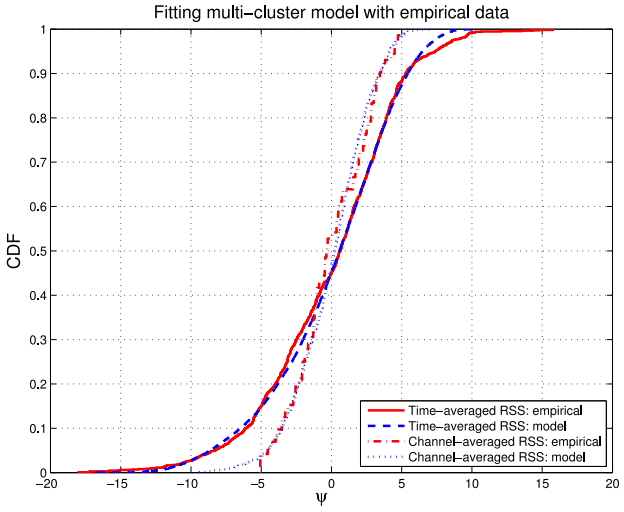

Fig. 15. Empirical and theoretical distributions of the RSS error. ROOM scenario.

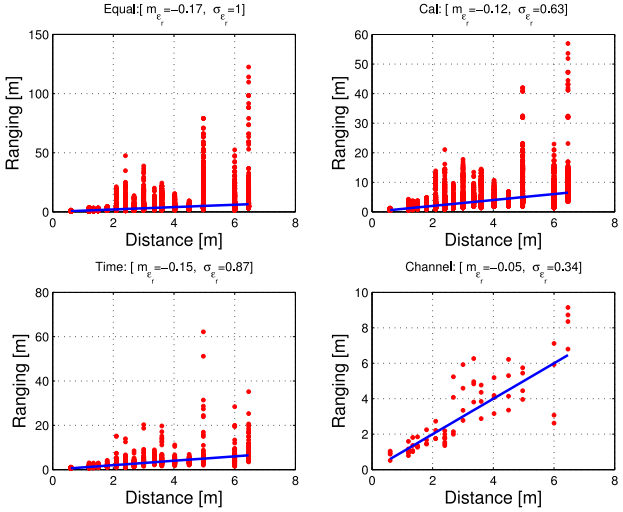

Fig. 16. Ranging estimate after successive refinement steps: offset compensation (upper-left), calibration (upper-right), time-averaging (lower-left), channel-averaging (lower-right). ROOM scenario.

Cluster delays τ_n were uniformly distributed in the interval $[t_0, t_{\max}]$, with $t_{\max} - t_0 \simeq 16$ ns, which is quite conservative in indoor environments [82], [106]. Fig. 15 compares the CDF of the error term Ψ obtained after time and frequency averaging of the RSS samples, respectively, both for the empirical and the simulated data. The good match of the empirical and theoretical distributions confirms the goodness of the multi-cluster propagation model for the considered environment, and the effectiveness of the multichannel RSS averaging technique to increase the accuracy of the RSS-based ranging.

X. RSS RANGING PERFORMANCE

The four refinement steps that can be applied to decrease the variance of the RSS measurements, namely offset compensation, calibration, time averaging and multichannel averaging, have also a positive effect in terms of ranging accuracy. In Fig. 16 we report the distance estimates (markers) obtained from the RSS values collected in the ROOM scenario, after each refinement step. The solid line represents the reference ground-truth distance. Note that the scale of the y-axis is varied in each graph to better appreciate the distribution of the ranging values. Above each graph we report the mean and standard deviation of the corresponding *relative* ranging error.

Observing the distribution of the RSS-based ranging values (markers) with respect to the actual distance (straight line), we can see that very large overestimates of the actual distance are quite likely to occur. However, each refinement step brings some improvement to the ranging accuracy, with the most significant gain given by the RSS calibration and the multichannel averaging.

To gain further insight on the impact of the different refinement steps on the ranging accuracy, we applied each of them in different combinations to the time-averaged RSS data collected on each testbed. The results are reported in Fig. 17, where we plot the module of the mean (upper graph) and the standard deviation (lower graph) of the relative ranging

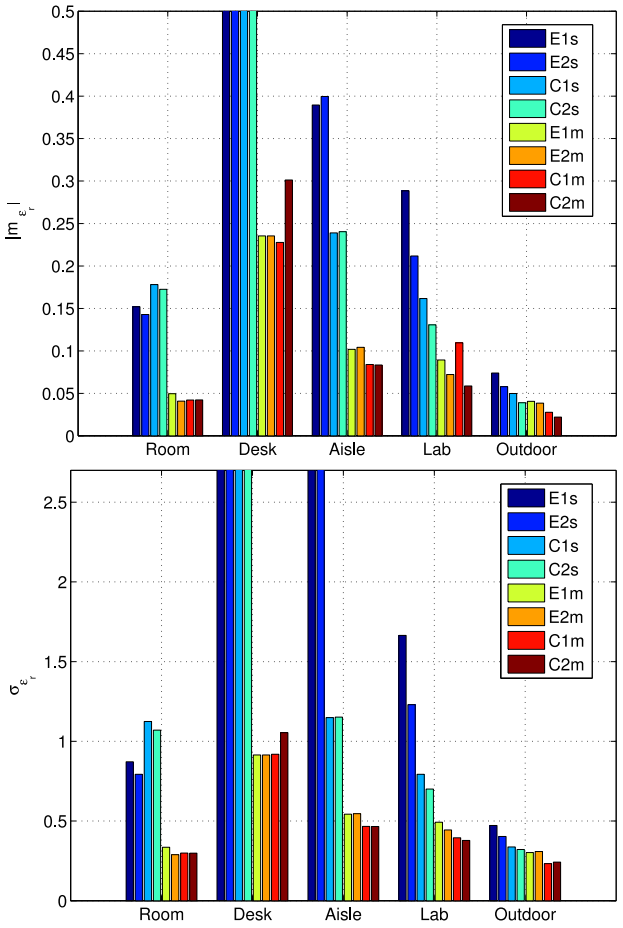

Fig. 17. Effect of the different refinement steps on the relative ranging error mean (upper) and standard deviation (lower) in the different scenarios. Symbols in the legend denote the refinement steps: `E/C`=equalized/calibrated RSS; `1/2`=one/two-slope pathloss model; `s/m`=single channel/multichannel average.

error, ε_r, defined by (15). Each bar corresponds to a different combination of the four refinement steps, as indicated in the figure's legend. The acronyms have the structure *Xmy*,

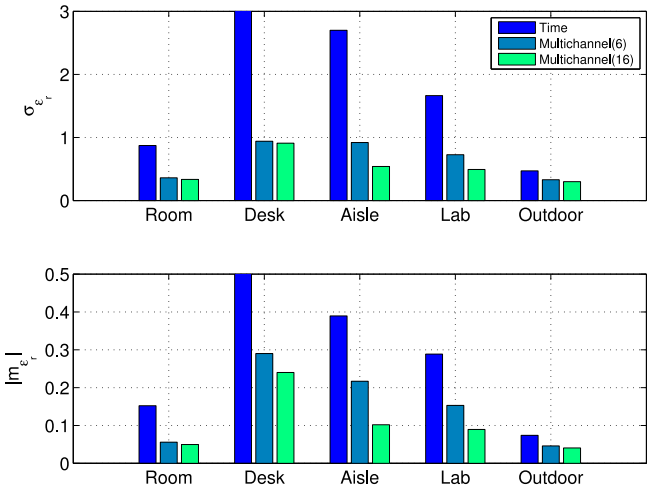

Fig. 18. Effect of time and frequency averaging on σ_{ε_r} (upper) and $|\mathrm{m}_{\varepsilon_r}|$ (lower). Groups of three bars refer to the different scenarios. In each group, the left, central and right bars refer to single-channel time-averaged RSS, and to frequency-averaged RSS over 6 and 16 channels, respectively.

where $X \in \{E, C\}$ stands for Equalized (E) or Calibrated (C), $m \in \{1, 2\}$ refers to the number of breakpoints in the path-loss model (4), and $y \in \{\mathrm{s}, \mathrm{m}\}$ indicates whether the RSS measurements have been considered for a single RF channel (s) or averaged over multiple RF channels (m). Therefore, the left-most bar of each group, labelled $E1s$, reports the results obtained by considering offset-equalized RSS data, with one-slope path-loss model (4), and single-channel RSS harvesting, which is the canonical situation considered in the largest part of the literature. The right-most bar ($C2m$), instead, refers to the results obtained from the same sets of RSS data, but using all the refinement steps described in this paper, i.e., RSS offset equalization, RSS calibration, two-slope path-loss model, and multichannel RSS averaging. Intermediate bars have been obtained by skipping one or two of these refinement steps.

We can immediately note that the multichannel RSS averaging is responsible for the most significant performance improvement in all the scenarios. Once performed multichannel RSS average, the other refinement steps bring negligible benefit. The only exception is represented by the outdoor scenario, where each refinement step brings a similar (but rather limited) improvement of the ranging accuracy, whose staring value (obtained with raw RSS measurements) is however much better than for the indoor scenarios.

At a closer look, we see that, when performing multichannel averaging, the RSS calibration is almost irrelevant, if not counterproductive as in the DESK scenario, probably because of the presence of the non-injective regions in the power-to-RSS transduction law $\mathcal{R}_\circ(\cdot)$.

From these results, we can conclude that multichannel RSS averaging is by far the most effective RSS refinement technique among those considered, in particular in harsh environments. The application of the other refinement techniques, such as calibration or multi-slope path-loss modeling, may bring some further performance improvement that, however, are rather limited.

It is then interesting to study how the RSS-based ranging performance is affected by the number of channels used for multichannel RSS averaging. To this end, we report in Fig. 18 the mean and standard deviation of ε_r for the different scenarios when averaging the RSS values over 1, 3, 6 and 16 RF-channels, equally spaced in the 80 MHz of the ISM band. We can observe that the multichannel averaging significantly decreases both $\mathrm{m}_{\varepsilon_r}$ and σ_{ε_r} in all the scenarios. Moreover, most of the performance gain is already achieved with as few as 6 different RF channels, provided that they are sufficiently spaced apart.

XI. RSS MEASUREMENTS IN OTHER CONDITIONS

The results presented in the previous sections have been mostly obtained from short-range wireless devices, in indoor and LOS conditions and with nodes at the same height. Yet, the methodological considerations that have been drawn upon such results have a wider scope and generally apply to other cases, which however, may also have their own peculiarities. In this section, we discuss some of the specificities that can be expected when the RSS measurements are collected in different conditions, included outdoor, non LOS, or with nodes at different heights.

An outdoor, long range scenario is considered, for example, in [109], where the authors present a detailed analysis of the statistical distribution of the signal strength in a GSM cellular system. The measurements have been performed at different carrier frequencies, when increasing the distance from the transmitting base station. The study shows that the shadowing terms, intended as the difference between the measured signal power and the reference value obtained from a classical single-slope path loss model, does not follow the canonical lognormal distribution but is better modeled by a *mixture of long-normal random variables*. Therefore, the MLE of the channel parameters shall be adjusted to account for such a particular distribution.

Another example is given in Fig. 19, where we report some data taken from the repository [110]. The experimental RSS samples were collected in an outdoor scenario, using WiFi. A WiFi wireless station (Bullet M2) was connected to a mobile robot, which moved along the trajectory shown in the upper-left quadrant of Fig. 19. While moving, the robot continuously sent WiFi packets to a stationary Access Point, placed at $X = -5$ m, $Y = 25$ m, $Z = 3.8$ m with respect to the robot's starting position, which recorded the RSS of each correctly decoded packet. The upper-right quadrant of Fig. 19 reports the actual RSS measurements collected for different distances of the robot from the Access Point, while the lower-left plot is obtained by applying a moving-average filter to the original data, with an averaging window that spans the RSS samples collected on an interval of approximately 6 cm. Finally, the lower-right plot shows the (average) RSS measurements obtained when the robot was covering the middle part of the trajectory (thick black line in the upper-left plot), thus remaining at a height from 9.1 m to 9.84 m. Each RSS plot also reports the parameters of the one-slope PLM obtained from (21).

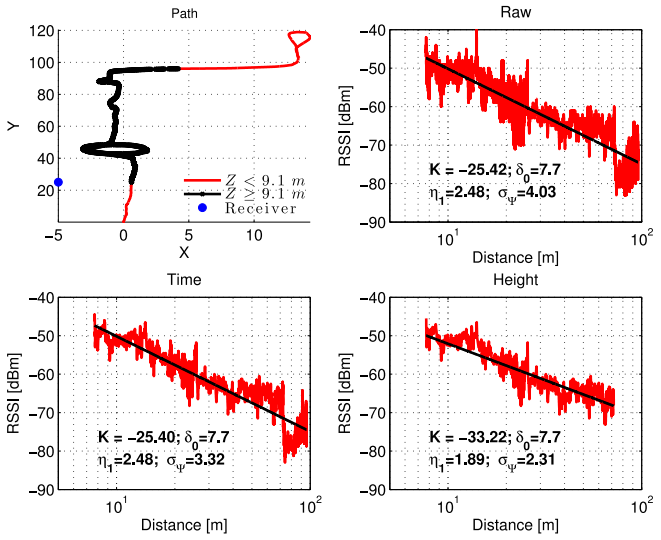

Fig. 19. Outdoor RSS measurements. Upper-left plot: planar path of the mobile transmitter; height Z varies from 8.1 m up to 9.84 m. Upper-right plot: RSS measurements at the receiver and estimated one-slope PLM. Lower-left plot: RSS measurements after time averaging. Lower-right plot: RSS measurements after time averaging and considering only points with $Z \geq 9.1$ m.

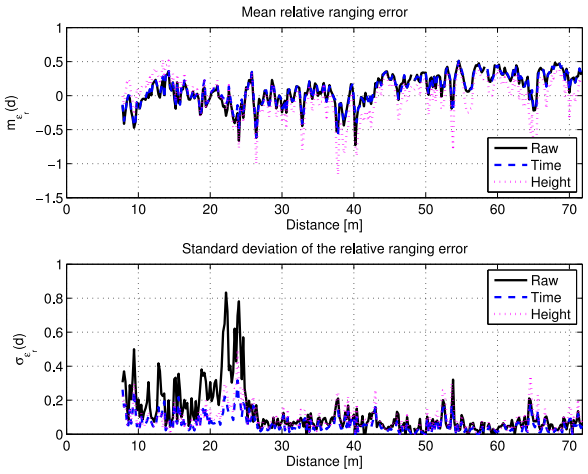

Fig. 20. Relative ranging error mean (upper) and standard deviation (lower) for the three cases of Fig. 19.

Observing the upper-right curves, we can note that the variability of the RSS measurements increases noticeably at a distance of about 20 m, where the transmitter makes a first loop, thus varying the angle between the transmitter and receiver antennas. A similarly effect can be noticed at $d \simeq 90$ m, in correspondence of the last loop in the trajectory. At a closer look, we could observe an average gap of about 5 dB between the RSS values collected in the forward and backward paths of each loop. This gap, too large to be ascribed to the path loss, is likely due to the asymmetric gain of the transmitter antenna, an asymmetry which can be intrinsic in the antenna design, or caused by coupling effects with the robot chassis, or a combination of the two factors. Hence, once again, the antenna radiation pattern has non negligible effect on the RSS measurements accuracy.

Another factor that can have a major impact on the quality of the RSS measurements is the distance from the ground/ceiling of the nodes antenna, since the presence of obstacles within the first Fresnel zone can result in severe attenuation/variability of the received signal strength [111]. It is indeed common experience that sensors lying directly on the ground, or close to it, have very short coverage range [36]. Furthermore, the antenna radiation pattern in the elevation plane can also have a major impact on the variability of the RSS measurements. This is particularly important when the height of the transmitter or receiver antenna changes during the RSS harvesting campaign, as in the example of Fig. 19. We can, in fact, notice a sudden drop of the RSS at a distance of about 80 m, when the robot starts moving downhill. Neglecting this variation of the height of the transmitter antenna has a negative effect on the estimation of the channel parameters, as can be appreciated by comparing the value of σ_Ψ reported in each of the RSS quadrants of Fig. 19, or the mean and variance of the relative ranging errors from Fig. 20.

A similar effect is experienced when passing from LOS to non LOS (NLOS) conditions. As observed in [112], the RSS in LOS conditions can be several dBs larger than in NLOS conditions, for the same distance. However, if LOS/NLOS condition can be correctly identified, then this information can greatly improve the performance of RSS-based indoor and outdoor localization [113]. Common approaches to discriminate LOS and NLOS conditions are based on the comparison of some key features of the empirical statistical distribution of the RSS samples, such as the mean and the standard deviation, the kurtosis (a measure of the peakedness of the probability density function), the skewness (a measure of the asymmetry of the probability distribution), the Rice factor, and so on [112]. These techniques, however, require a rather accurate estimate of the statistical distribution of the RSS measurements for the different distances that, in turn, requires a large number of measurements.

Finally, channel parameters may be non-stationary because of the nodes mobility or mid-to-long term changes in the environment [95], [114]. As shown in [93], the uncertainty in the estimation of the PLM parameters yields a statistical bias in the estimated distance, with negative effect on the localization. Still in [93], it is proved that such a bias can be mitigated, but this requires the anchors to be properly placed. Another study on RSS-based localization in non-homogeneous environments is presented in [115], where the authors propose a two-stage procedure consisting first in the estimation of the attenuation factors among the anchors and, then, in the application of a maximum likelihood localization algorithm to estimate the unknown position of the blind wireless node.

XII. Conclusion

In this tutorial paper we have reviewed the most common approaches to obtain ranging estimates from the measurements of the radio signal power received by a wireless node. Starting from a thorough analysis of the reference channel model used to describe the decay of the radio signal with the travelled distance, we have then considered one by one the different

steps that are generally performed to obtain a distance estimate from a vector of raw RSS measurements. Hence, we verified the impact of the different operations on the accuracy of the channel parameters estimate and the relative ranging performance.

To wrap up the discussion, we here summarize some fundamental lessons that can be learned from our study and, then, discuss some possible research directions, open issues and challenges.

A. Good Practice Recommendations

1) Calibration of RSS Readings: The granularity of the power-to-RSS transduction law is totally negligible. Instead, non-linearities and offsets in the power-to-RSS functions may have a severe impact on the accuracy of the RSS measurements. It is hence recommended to compensate the RSS offset and, whenever possible, to rectify the transduction law of the different nodes (in this order).

A way to exactly estimate the RSS offset of a node is to attach a signal generator to the connector of the external antenna, and transmit a signal with known power. The difference between the actual and expected RSS readings is equal to the RSS offset of the circuit, which can then be compensated by properly setting an internal register of the wireless board, or simply subtracting the estimated offset to all the RSS readings of that node.

A simpler (but slightly less accurate) procedure to estimate the *relative* offset between two nodes is described in Section VI-C, and consists in exchanging a number of two-way packets between the nodes and computing the mean difference between the respective RSS readings. If one node has zero offset, this process makes it possible to estimate and compensate the offset of the other node. Otherwise, it can be used to simply harmonize the offsets of the different nodes to a common value. Note that the rectification of the RSS transduction law is meaningful only when the offsets have been compensated.

2) Antenna Anisotropy: The antenna radiation patterns are often overlooked, but they can strongly affect the performance of the RSS-based ranging. In particular, the radiation pattern of patch antennas may be quite irregular, with several dBs of difference depending on the angle. Clearly, such variations may have a dramatic impact on the accuracy of the RSS-based ranging.

Practitioners are hence recommended to take into account the actual radiation patterns of their devices, for example by orienting the anchor nodes so that the maximum gain lobe is turned towards the monitored area. Furthermore, the nodes shall be placed at the same height, to mitigate the vertical asymmetries of the radiation pattern of the antenna.

If the nodes can be rotated around their axis, it is possible to collect multiple RSS samples with different relative orientations of the antennas. Knowing the nominal radiation pattern of the antenna, it is then possible to estimate the orientations of the nodes and, then, compensate the difference of the antenna gains. These procedures, however, may be unfeasible or very cumbersome in practical settings. Therefore, the use of (external) isotropic antenna is strongly recommended.

3) Short-Term Fading: The fast fading term that affects the RSS samples can be smoothed out by averaging a few RSS samples, say from 10 to 15, sufficiently spaced apart in time to decorrelate the fast fading coefficients. Increasing the number of samples over 15 is not much convenient, since the reduction of the fast-fading noise is very limited and may not justify the extra energy and time costs incurred in the collection of the additional RSS samples.

The time average can be performed directly on the values in dB scale (as typically returned by the RSS register), or by first converting the readings in linear scale. The last approach is preferable because the result is unbiased and exhibits slightly lower variance.

4) Path Loss Model: The estimate of the PLM parameters also requires some care. First of all, piece-wise PLMs shall be considered, in particular when the distances are relatively small (order of meters). However, a two-slope model is typically sufficient, while models with more than three slopes are discouraged because of the risk of overfitting. Second, attention shall be devoted to avoid any bias due to the sensitivity threshold of the receiver, which may become relevant at large distances, close to the reception range of the devices.

5) Long-Term Fading: Despite the long-term fading that affects the RSS samples is often associated to shadowing phenomena and modeled as a lognormal random variable (in linear scale), in indoor environment it may be strongly contributed by the self-interference produced by few clusters of strong signal reflections. In this case, the statistical distribution is better captured by other models, such as the Extreme Value distribution (see the Appendix). Using the most proper statistical model for the long-term fading may help improving the accuracy of the channel parameters estimate.

The component of the long-term fading coefficients due to the self-interference can be dramatically reduced by averaging multiple RSS samples collected over different RF channels. Indeed, the spatial diversity obtained by changing the carrier frequency is sufficient to partially decorrelate the phases of the reflected signals, as better explained in [96]. The mean RSS values obtained after multichannel averaging, furthermore, exhibit a statistical distribution which is closer to the canonical lognormal model, which means that the error term in (18) is gaussian and, hence, the MSE estimate given by (21) actually corresponds to the maximum likelihood estimate of the channel parameters.

It is therefore highly recommended to average multiple RSS samples collected on different RF channels, widely spaced apart. Note that, in this way, we not only mitigate the long-term fading, but also reduce the fast-fading term, since the RSS samples will also be distributed in time. The multichannel RSS averaging is by far the most effective way to improve the accuracy of RSS-based ranging among those analyzed in this paper. However, the information contained in multi-channel RSS samples can be better exploited by using other, more sophisticated techniques, as those proposed in [104] and [105].

6) Summing Up: We can hence conclude that obtaining an accurate measurements of the received signal power, or a good ranging estimate, by using RSS measurements is indeed a challenging endeavor. However, the awareness of the factors

that affect the accuracy of the RSS measurements can help to avoid some trivial mistakes. In particular, the calibration of the RSS circuits to remove the RSS offsets, the use of isotropic antennas, and the averaging of RSS samples over different carrier frequencies have been identified as the most important elements to enhance the accuracy of the RSS-based ranging.

B. Discussion

Our review of the most common approaches to collect RSS measurements, and the related pitfalls, may suggest some new design criteria for wireless devices that can natively support accurate RSS measurements and/or ranging and new methodologies to improve the quality of the RSS-based ranging estimation techniques.

For example, an anisotropic and asymmetric radiation pattern, which may severely affect the reliability of classical RSS-based ranging, can be exploited to infer the mutual orientation of the transmitter and receiver antennas, thus making it possible to compensate the different antenna gains and providing an extremely valuable information for node tracking algorithms. Therefore, the design and testing of practical and effective algorithms to determine the node's orientation are open and interesting research problems.

Another research direction that has not yet been fully investigated regards the calibration of the nodes' sensors to compensate offsets and non-idealities. A possible solution consists in applying consensus techniques to reach a global agreement on the settings of the tuneable parameters (e.g., RSS offset, time reference, transmit power) among the nodes in the network. However, these technique are rather costly in terms of energy consumption, control traffic, and convergence time. Therefore, further research is needed to find lighter algorithms/procedures to compensate the unavoidable offsets of the nodes' sensors.

From a methodological perspective, a promising approach consists in departing from the classic PLM to investigate alternative statistical models for the received signal power, in order to better account for the environmental variability. An example is given in [116], where the authors propose a Bayesian model for the received power, which is represented as the sum of two random terms, one for the distance-dependent power attenuation and the other for the fading component. The statistical distribution of the first random variable is parametric and, hence, can capture different environmental conditions as, for instance, the presence or absence of LOS. The authors then propose a relatively simple way to obtain a ranging estimate from the RSS readings by using Bayesian estimation. The simulation results obtained in a test scenario show that the proposed approach can outperform the classical PLM-inversion ranging methods, thus suggesting that more sophisticated RSS models can help to improve the accuracy of the received power measurements and of the RSS-based ranging.

Another interesting approach is proposed in [117], where a particle filter is used to select the best RSS measurements and improve the accuracy of RSS-based ranging even in the presence of mixed LOS/NLOS conditions and for different attenuation factors and fading levels. Furthermore, the ranging accuracy is improved by considering geometric constraints that can be obtained using other techniques, such as the difference time of arrival among the different anchors.

Other still largely unexplored research avenues include the development and experimental analysis of algorithms and techniques for efficient and accurate RSS harvesting in mobile networks, the use of cooperative and opportunistic techniques to improve the localization accuracy of the different nodes [118], [119], and the exploitation of other types of signal for ranging as, for example, visible light [120].

As a final comment, we observe that the huge and variegate literature on the subject, and the availability of a number of commercial products that can provide RSS measurements and radio-based ranging and localization services, have not yet exhausted the interest of these topics for the scientific community, an interest that has instead been renovated by the advent of new technologies, such as low power wide area network standards (e.g., SigFox, LoRa, Ingenu) and millimeter waves, new communication paradigms, as machine-type communication and vehicular communication, and new application scenarios, as Internet of Things and Smart Cities [121]. Accurate RSS measurements, distance estimation, and localization/tracking of the nodes in the network are, indeed, extremely valuable information to be used for the optimization of the network management, e.g., by enabling the design of position-aware scheduling algorithms in interference-limited systems, or the deployment of efficient in-network data compression/fusion techniques based on the spatial correlation of the sensor measurements, or the improvement of energy efficiency of machine-type devices by channel-aware scheduling and rate adaptation algorithms. Therefore, squeezing out information from RSS measurements will likely remain an attractive research and engineering challenge for yet some years to come.

APPENDIX

A. Long-Term Fading Models

In principle, the long-term fading accounts for the space variability of the received signal power due to the variations of the number and typology of obstructing surfaces along the path followed by the radio signal from the transmitter to the receiver [78], [82]. If the signal path goes through many obstructing objects of different size and material, the overall attenuation (in dB scale) can be approximated to a Gaussian random variable, which gives a lognormal random variable in linear scale and motivates the name *lognormal shadowing* commonly used to refer to this model. The lognormal shadowing has been empirically observed in many scenarios, in particular when considering *global* data (measurements collected over a large area), or even *local* data (measurements collected by a couple of nodes in a fixed position) in the case of obstructed paths [82].

Another possible model for the long-term fading is the *Weibull model* [103], according to which Ψ_{LN} is characterized by the PDF

$$f_{\Psi_{\text{LN}}}(x) = \frac{\beta}{\lambda^{\beta}} x^{\beta-1} e^{-(x/\lambda)^{\beta}}, \tag{25}$$

where $\lambda > 0$ is called *scale parameter*, and $\beta > 0$ *shape parameter*. Since Ψ_{LN} has unit mean, it holds $\lambda = 1/\Gamma(1+\frac{1}{\beta})$, where $\Gamma(x) = \int_0^\infty e^{-a}a^{x-1}\mathrm{d}a$ is the Gamma function. Therefore, the distribution of Ψ_{LN} is governed by the parameter β only. The Weibull distribution is a special case of the α-μ distribution [79], more commonly known as Generalized Gamma (or Stacy) distribution [79], and it interpolates between the exponential distribution ($\beta = 1$) and the Rayleigh distribution ($\beta = 2$).

If Ψ_{LN} is Weibull distributed, then Ψ has *Extreme Value* distribution, whose PDF is given by

$$f_\Psi(x) = \frac{1}{\sigma} e^{\frac{x-\mu}{\sigma} - e^{\frac{x-\mu}{\sigma}}}, \tag{26}$$

where $\mu = \xi \ln(\mu) = 10\log(\lambda)$ and $\sigma = \frac{\xi}{\beta}$. In this case, the statistical mean of Ψ turns out to be equal to

$$\mathrm{m}_\Psi = \mu - \sigma\gamma_0$$

where γ_0 is the Euler-Mascheroni constant. Therefore, the mean of the shadowing term in dB scale is non-zero even when Ψ_{LN} has unit mean in linear scale.

B. Rician Fading Model

Let $h(t, \mathbf{s})$ denote the complex equivalent channel impulse response and let $\gamma(t, \mathbf{s}) = |h(t, \mathbf{s})|^2$ be its squared envelope. The short-term fading in linear scale, $a_{\text{LN}}(t)$, can hence be defined as

$$a_{\text{LN}}(t) = \frac{\gamma(t, \mathbf{s})}{\bar{\gamma}(\mathbf{s})}; \tag{27}$$

where $\bar{\gamma}(\mathbf{s})$ is the ergodic time average of the channel gain. Therefore, $a_{\text{LN}}(t)$ has unit time average by construction, i.e.,

$$\mathrm{m}_{a_{\text{LN}}} = \mathrm{E}\big[a_{\text{LN}}(t)\big] = 1.$$

According to the Rician fading model, we hence have $h(t, \mathbf{s}) = X + jY$, where X and Y are mutually uncorrelated normal random processes with mean m_X and m_Y and equal variance σ_t^2 [82]. Therefore, the module $|h(\mathbf{s}, t)| = \sqrt{\gamma(t, \mathbf{s})} = \sqrt{X^2 + Y^2}$ is distributed as a Rice random variable, with Rice Factor $R_F = \frac{\mathrm{m}_X^2 + \mathrm{m}_Y^2}{2\sigma_t^2}$, and overall signal power $\bar{\gamma}(\mathbf{s}) = \mathrm{m}_X^2 + \mathrm{m}_Y^2 + 2\sigma_t^2 = 2\sigma_t^2(R_F + 1)$. From (27) we then have

$$a_{\text{LN}}(t) = \frac{(X^2 + Y^2)/\sigma_t^2}{2(R_F + 1)} = \frac{\zeta}{2(R_F + 1)}; \tag{28}$$

where ζ is a non-central chi-square distributed random variable with two degrees of freedom and non centrality parameter $\nu = \frac{\mathrm{m}_X^2 + \mathrm{m}_Y^2}{\sigma_t^2} = 2R_F$. The variance of $a_{\text{LN}}(t)$ is equal to

$$\sigma^2_{a_{\text{LN}}} = \frac{\sigma^2_\zeta}{4(R_F + 1)^2} = \frac{4(2R_F + 1)}{4(R_F + 1)^2} = \frac{2R_F + 1}{(R_F + 1)^2}.$$

C. Averaging Short-Term Fading

1) Time Averaging in Linear Scale: Taking the average of N short-term fading samples in linear scale, sufficiently spaced apart in time to be uncorrelated, we get

$$\bar{a}_{\text{LN}}(N) = \frac{1}{N}\sum_{i=1}^{N} a_{\text{LN}}(t_i);$$

which is an Erlang-distributed random variable, with shape parameter N, and rate parameter $\lambda = 1$. Converting the result in dB scale we obtain

$$\bar{a}(N) = 10\log\big(\bar{a}_{\text{LN}}(N)\big) = \xi \ln(\bar{a}_{\text{LN}}(N)); \tag{29}$$

where $\xi = 10\log(e)$. The statistical mean and variance of (29) turn out to be equal to

$$\begin{aligned} \mathrm{m}_{\bar{a}(N)} &= \xi(\mathrm{PoliG}_0(N) - \ln(N)); \\ \sigma^2_{\bar{a}(N)} &= \xi^2 \mathrm{PoliG}_1(N); \end{aligned} \tag{30}$$

respectively. In (30), $\mathrm{PoliG}_m(k)$ represents the *polygamma* function of order m that, in our case, is given by the $(m+1)$st derivative of the logarithm of the factorial $k!$.

2) Time Averaging in dB Scale: Averaging N samples in dB scale we get

$$\overline{a(N)} = \frac{1}{N}\sum_{i=1}^{n} a(t_i); \tag{31}$$

where $a(t_i)$ is distributed as $\bar{a}(1)$ in (29). The mean and variance of $\overline{a(N)}$ are

$$\begin{aligned} \mathrm{m}_{\overline{a(N)}} &= \mathrm{m}_{\bar{a}_1^{\text{dB}}} = -\xi\gamma; \\ \sigma^2_{\overline{a(N)}} &= \frac{\sigma^2_{\bar{a}_1^{\text{dB}}}}{N} = \xi^2\frac{\pi^2}{6N}; \end{aligned} \tag{32}$$

where γ is the Euler-Mascheroni constant. We can then observe that averaging the value in dB scale yields a constant, negative bias, which can be easily compensated for or included in the deterministic term $\mathcal{K}$ of the PLM (6), while the variance of the average decreases linearly with N.

D. Finding the Critical Distance d°

Let $P_{ok}(x)$ be the successful packet reception probability when the received signal power (in dB scale) is x. Then, the PDF of $\mathring{\Psi}$ can be expressed as the conditional PDF of Ψ, given that the packet is successfully decoded, i.e.,

$$f_{\mathring{\Psi}}(a) = \frac{f_\Psi(a)P_{ok}(D(d) + a)}{\int_{-\infty}^{\infty} f_\Psi(v)P_{ok}(D(d) + v)\mathrm{d}v}. \tag{33}$$

To simplify the analysis we approximate $P_{ok}(x)$ as the unit-step function $H(x - \Gamma_{\texttt{thr}})$, so that a packet is successfully decoded only when the received signal power is above a certain threshold $\Gamma_{\texttt{thr}}$. In this case, (33) becomes

$$f_{\mathring{\Psi}}(a) = \frac{f_\Psi(a)}{1 - F_\Psi(\Gamma_{\texttt{thr}} - D(d))}, \quad a \geq 0, \tag{34}$$

where $F_\Psi(\cdot)$ denotes the Cumulative Distribution Function (CDF) of the random variable Ψ. When the denominator of (34) gets close to one, the PDF of $\mathring{\Psi}$ tends to that of Ψ, which is distance-independent. Therefore, given a positive $\epsilon \ll 1$, we can find the maximum distance d° within which $\mathring{\Psi}$ has approximately the same distribution as Ψ, i.e.,

$$d^\circ = \arg\max_d \{F_\Psi(\Gamma_{\texttt{thr}} - D(d)) \leq \epsilon\}. \tag{35}$$

Unfortunately, the term $D(d)$ in (35) intertwines the estimate of d° with that of the channel parameters, so that it is necessary to solve (35) in a recursive manner: we first set $d^\circ = \infty$

and estimate the PLM parameters under the assumption that the consider shadowing model is valid. Then, we evaluate (35) to obtain a new value of d°, using the just estimated channel parameters, and verify *a posteriori* whether all the RSS samples used in the estimate where collected at distances less than d°. If not, the procedure is repeated by considering only the RSS values collected at distances $d_i \leq d^{\circ}$, until the condition is satisfied.

ACKNOWLEDGMENT

Author wish to acknowledge Dr. Francesco Zorzi and Dr. Andrea Bardella for their contribution in collecting the RSS measurements used in this work.

REFERENCES

[1] Y. Liu, Z. Yang, X. Wang, and L. Jian, "Location, localization, and localizability," *J. Comput. Sci. Technol.*, vol. 25, no. 2, pp. 274–297, 2010.

[2] T. He, C. Huang, B. M. Blum, J. A. Stankovic, and T. Abdelzaher, "Range-free localization schemes for large scale sensor networks," in *Proc. 9th Annu. Int. Conf. Mobile Comput. Netw.*, San Diego, CA, USA, 2003, pp. 81–95.

[3] B. Dil, S. Dulman, and P. Havinga, "Range-based localization in mobile sensor networks," in *Wireless Sensor Networks*. Heidelberg, Germany: Springer, 2006, pp. 164–179.

[4] S. P. Singh and S. C. Sharma, "Range free localization techniques in wireless sensor networks: A review," *Proc. Comput. Sci.*, vol. 57, pp. 7–16, 2015. [Online]. Available: http://www.sciencedirect.com/science/article/pii/S1877050915018864

[5] H. Liu, H. Darabi, P. Banerjee, and J. Liu, "Survey of wireless indoor positioning techniques and systems," *IEEE Trans. Syst., Man, Cybern. C, Appl. Rev.*, vol. 37, no. 6, pp. 1067–1080, Nov. 2007.

[6] N. Bulusu, J. Heidemann, and D. Estrin, "GPS-less low-cost outdoor localization for very small devices," *IEEE Pers. Commun.*, vol. 7, no. 5, pp. 28–34, Oct. 2000.

[7] D. Niculescu and B. Nath, "DV based positioning in ad hoc networks," *Telecommun. Syst.*, vol. 22, nos. 1–4, pp. 267–280, 2003.

[8] Y. Wang, X. Wang, D. Wang, and D. P. Agrawal, "Range-free localization using expected hop progress in wireless sensor networks," *IEEE Trans. Parallel Distrib. Syst.*, vol. 20, no. 10, pp. 1540–1552, Oct. 2009.

[9] Y. Shang, W. Ruml, Y. Zhang, and M. P. J. Fromherz, "Localization from mere connectivity," in *Proc. 4th ACM Int. Symp. Mobile Ad Hoc Netw. Comput.*, Annapolis, MD, USA, 2003, pp. 201–212.

[10] L. Doherty, K. S. J. Pister, and L. El Ghaoui, "Convex position estimation in wireless sensor networks," in *Proc. IEEE INFOCOM*, vol. 3. Anchorage, AK, USA, 2001, pp. 1655–1663.

[11] P. Bahl and V. N. Padmanabhan, "RADAR: An in-building RF-based user location and tracking system," in *Proc. INFOCOM*, vol. 2. Tel Aviv, Israel, 2000, pp. 775–784.

[12] L. Gogolak, S. Pletl, and D. Kukolj, "Indoor fingerprint localization in WSN environment based on neural network," in *Proc. IEEE 9th Int. Symp. Intell. Syst. Informat. (SISY)*, Subotica, Serbia, 2011, pp. 293–296.

[13] M. Bshara, U. Orguner, F. Gustafsson, and L. Van Biesen, "Fingerprinting localization in wireless networks based on received-signal-strength measurements: A case study on WiMAX networks," *IEEE Trans. Veh. Technol.*, vol. 59, no. 1, pp. 283–294, Jan. 2010.

[14] Y. Chapre, P. Mohapatra, S. Jha, and A. Seneviratne, "Received signal strength indicator and its analysis in a typical WLAN system (short paper)," in *Proc. IEEE Conf. Local Comput. Netw. (LCN)*, Sydney, NSW, Australia, Oct. 2013, pp. 304–307.

[15] A. Savvides, H. Park, and M. B. Srivastava, "The n-hop multilateration primitive for node localization problems," *Mobile Netw. Appl.*, vol. 8, no. 4, pp. 443–451, 2003.

[16] A. Savvides, H. Park, and M. B. Srivastava. (2002). *The Bits and Flops of the n-Hop Multilateration Primitive for Node Localization Problems*. [Online]. Available: http://citeseer.ist.psu.edu/savvides02bits.html

[17] S. Salari, S. ShahbazPanahi, and K. Ozdemir, "Mobility-aided wireless sensor network localization via semidefinite programming," *IEEE Trans. Wireless Commun.*, vol. 12, no. 12, pp. 5966–5978, Dec. 2013.

[18] G. Wang and K. Yang, "A new approach to sensor node localization using RSS measurements in wireless sensor networks," *IEEE Trans. Wireless Commun.*, vol. 10, no. 5, pp. 1389–1395, May 2011.

[19] P. Biswas, T.-C. Lian, T.-C. Wang, and Y. Ye, "Semidefinite programming based algorithms for sensor network localization," *ACM Trans. Sensor Netw.*, vol. 2, no. 2, pp. 188–220, May 2006.

[20] N. Patwari, III, A. O. Hero, M. Perkins, N. S. Correal, and R. J. O'Dea, "Relative location estimation in wireless sensor networks," *IEEE Trans. Signal Process.*, vol. 51, no. 8, pp. 2137–2148, Aug. 2003.

[21] I. Guvenc, S. Gezici, F. Watanabe, and H. Inamura, "Enhancements to linear least squares localization through reference selection and ML estimation," in *Proc. IEEE Wireless Commun. Netw. Conf. (WCNC)*, Las Vegas, NV, USA, 2008, pp. 284–289.

[22] M. Grey, M. Rossberg, M. Backhaus, and G. Schaefer, "On distributed geolocation by employing spring-mass systems," in *Proc. IEEE Glob. Inf. Infrastruct. Symp.*, Trento, Italy, 2013, pp. 1–7.

[23] K. Heurtefeux and F. Valois, "Is RSSI a good choice for localization in wireless sensor network?" in *Proc. IEEE 26th Int. Conf. Adv. Inf. Netw. Appl. (AINA)*, Fukuoka, Japan, Mar. 2012, pp. 732–739.

[24] N. B. Priyantha, H. Balakrishnan, E. Demaine, and S. Teller, "Anchor-free distributed localization in sensor networks," in *Proc. 1st Int. Conf. Embedded Netw. Sensor Syst.*, Los Angeles, CA, USA, 2003, pp. 340–341.

[25] J. Sallai, G. Balogh, M. Maroti, A. Ledeczi, and B. Kusy, "Acoustic ranging in resource-constrained sensor networks," in *Proc. Int. Conf. Wireless Netw.*, Las Vegas, NV, USA, 2004, p. 467.

[26] S. E. Reutebuch, H.-E. Andersen, and R. J. McGaughey, "Light detection and ranging (LIDAR): An emerging tool for multiple resource inventory," *J. Forest.*, vol. 103, no. 6, pp. 286–292, 2005.

[27] B. Thorbjornsen, N. M. White, A. D. Brown, and J. S. Reeve, "Radio frequency (RF) time-of-flight ranging for wireless sensor networks," *Measur. Sci. Technol.*, vol. 21, no. 3, 2010, Art. no. 035202.

[28] T. Erseghe, S. Tomasin, and A. Vigato, "Topology estimation for smart micro grids via powerline communications," *IEEE Trans. Signal Process.*, vol. 61, no. 13, pp. 3368–3377, Jul. 2013.

[29] S. Lanzisera, D. T. Lin, and K. S. J. Pister, "RF time of flight ranging for wireless sensor network localization," in *Proc. IEEE Int. Workshop Intell. Solut. Embedded Syst.*, Vienna, Austria, 2006, pp. 1–12.

[30] N. B. Priyantha, A. Chakraborty, and H. Balakrishnan, "The cricket location-support system," in *Proc. 6th Annu. Int. Conf. Mobile Comput. Netw. (MobiCom)*, Boston, MA, USA, 2000, pp. 32–43.

[31] I. Guvenc and C.-C. Chong, "A survey on TOA based wireless localization and NLOS mitigation techniques," *IEEE Commun. Surveys Tuts.*, vol. 11, no. 3, pp. 107–124, Sep. 2009.

[32] D. Li, K. D. Wong, Y. H. Hu, and A. M. Sayeed, "Detection, classification, and tracking of targets," *IEEE Signal Process. Mag.*, vol. 19, no. 2, pp. 17–29, Mar. 2002.

[33] G. Zanca, F. Zorzi, A. Zanella, and M. Zorzi, "Experimental comparison of RSSI-based localization algorithms for indoor wireless sensor networks," in *Proc. Workshop Real World Wireless Sensor Netw.*, Glasgow, Scotland, 2008, pp. 1–5.

[34] A. Bardella, N. Bui, A. Zanella, and M. Zorzi, "An experimental study on IEEE 802.15.4 multichannel transmission to improve RSSI-based service performance," in *Real-World Wireless Sensor Networks*. Heidelberg, Germany: Springer, 2010, pp. 154–161.

[35] A. Coluccia and F. Ricciato, "A software-defined radio tool for experimenting with RSS measurements in IEEE 802.15.4: Implementation and applications," *Int. J. Sensor Netw.*, vol. 14, no. 3, pp. 144–154, 2013.

[36] K. Whitehouse, C. Karlof, and D. Culler, "A practical evaluation of radio signal strength for ranging-based localization," *ACM SIGMOBILE Mobile Comput. Commun. Rev.*, vol. 11, no. 1, pp. 41–52, 2007.

[37] F. D. Rosa, M. Pelosi, and J. Nurmi, "Human-induced effects on RSS ranging measurements for cooperative positioning," *Int. J. Navig. Observation*, vol. 2012, 2012, Art. no. 959140, doi: 10.1155/2012/959140.

[38] G. Han, H. Xu, T. Q. Duong, J. Jiang, and T. Hara, "Localization algorithms of wireless sensor networks: A survey," *Telecommun. Syst.*, vol. 52, no. 4, pp. 2419–2436, 2013.

[39] N. Patwari *et al.*, "Locating the nodes: Cooperative localization in wireless sensor networks," *IEEE Signal Process. Mag.*, vol. 22, no. 4, pp. 54–69, Jul. 2005.

[40] K. P. Subbu, C. Zhang, J. Luo, and A. V. Vasilakos, "Analysis and status quo of smartphone-based indoor localization systems," *IEEE Wireless Commun.*, vol. 21, no. 4, pp. 106–112, Aug. 2014.

[41] G. Sun, J. Chen, W. Guo, and K. J. R. Liu, "Signal processing techniques in network-aided positioning: A survey of state-of-the-art positioning designs," *IEEE Signal Process. Mag.*, vol. 22, no. 4, pp. 12–23, Jul. 2005.

[42] A. Awad, T. Frunzke, and F. Dressler, "Adaptive distance estimation and localization in WSN using RSSI measures," in *Proc. 10th Euromicro Conf. Digit. Syst. Design Architect. Methods Tools (DSD)*, Lübeck, Germany, 2007, pp. 471–478.

[43] M. B. Ayed and A. B. Ayed, "Systems for wireless authentication based on bluetooth proximity," U.S. Patent 8 045 961, Oct. 25, 2011.

[44] X. Lin, J. G. Andrews, A. Ghosh, and R. Ratasuk, "An overview of 3GPP device-to-device proximity services," *IEEE Commun. Mag.*, vol. 52, no. 4, pp. 40–48, Apr. 2014.

[45] J. Hightower and G. Borriello, "Location systems for ubiquitous computing," *Computer*, vol. 34, no. 8, pp. 57–66, 2001.

[46] A. Bardella, N. Bui, A. Zanella, and M. Zorzi, "Constrained localization: Mapping wireless sensor nodes in predefined positions," in *Proc. IEEE Glob. Telecommun. Conf. (GLOBECOM)*, Houston, TX, USA, 2011, pp. 1–5.

[47] N. Patwari and A. O. Hero, III, "Using proximity and quantized RSS for sensor localization in wireless networks," in *Proc. 2nd ACM Int. Conf. Wireless Sensor Netw. Appl.*, San Diego, CA, USA, 2003, pp. 20–29.

[48] P. Kumar, L. Reddy, and S. Varma, "Distance measurement and error estimation scheme for RSSI based localization in wireless sensor networks," in *Proc. IEEE Conf. Wireless Commun. Sensor Netw. (WCSN)*, Allahabad, India, 2009, pp. 1–4.

[49] G. Blumrosen, B. Hod, T. Anker, D. Dolev, and B. Rubinsky, "Enhancing RSSI-based tracking accuracy in wireless sensor networks," *ACM Trans. Sensor Netw.*, vol. 9, no. 3, 2013, Art. no. 29.

[50] M. A. Caceres, F. Sottile, and M. A. Spirito, "Adaptive location tracking by Kalman filter in wireless sensor networks," in *Proc. IEEE Int. Conf. Wireless Mobile Comput. Netw. Commun. (WIMOB)*, Marrakesh, Morocco, Oct. 2009, pp. 123–128.

[51] K.-C. Lee, A. Oka, E. Pollakis, and L. Lampe, "A comparison between unscented Kalman filtering and particle filtering for RSSI-based tracking," in *Proc. Workshop Positioning Navig. Commun. (WPNC)*, Dresden, Germany, 2010, pp. 157–163.

[52] A. S. Paul and E. A. Wan, "RSSI-based indoor localization and tracking using sigma-point Kalman smoothers," *IEEE J. Sel. Topics Signal Process.*, vol. 3, no. 5, pp. 860–873, Oct. 2009.

[53] Y.-H. Choi, T.-K. Lee, and S.-Y. Oh, "A line feature based SLAM with low grade range sensors using geometric constraints and active exploration for mobile robot," *Auton. Robots*, vol. 24, no. 1, pp. 13–27, 2008.

[54] S. Ahn, J. Choi, N. L. Doh, and W. K. Chung, "A practical approach for EKF-SLAM in an indoor environment: Fusing ultrasonic sensors and stereo camera," *Auton. Robots*, vol. 24, no. 3, pp. 315–335, 2008.

[55] E. Menegatti, A. Zanella, S. Zilli, F. Zorzi, and E. Pagello, "Range-only SLAM with a mobile robot and a wireless sensor networks," in *Proc. IEEE Int. Conf. Robot. Autom. (ICRA)*, Kobe, Japan, 2009, pp. 8–14.

[56] E. Menegatti *et al.*, "Autonomous discovery, localization and recognition of smart objects through WSN and image features," in *Proc. IEEE GLOBECOM Workshops*, Miami, FL, USA, 2010, pp. 1653–1657.

[57] A. Bardella *et al.*, "Autonomous robot exploration in smart environments exploiting wireless sensors and visual features," *Ann. Telecommun. Annales Des Télécommunications*, vol. 67, nos. 7–8, pp. 297–311, 2012.

[58] S. Wu, S. Biaz, and H. Wang, "Rate adaptation with loss diagnosis on IEEE 802.11 networks," *Int. J. Commun. Syst.*, vol. 25, no. 4, pp. 515–528, 2012.

[59] G. Judd, X. Wang, and P. Steenkiste, "Efficient channel-aware rate adaptation in dynamic environments," in *Proc. 6th Int. Conf. Mobile Syst. Appl. Services*, Breckenridge, CO, USA, 2008, pp. 118–131.

[60] N. Baldo *et al.*, "Gora: Goodput optimal rate adaptation for 802.11 using medium status estimation," in *Proc. IEEE Int. Conf. Commun. (ICC)*, Beijing, China, 2008, pp. 4916–4921.

[61] G. Holland, N. Vaidya, and P. Bahl, "A rate-adaptive MAC protocol for multi-hop wireless networks," in *Proc. 7th Annu. Int. Conf. Mobile Comput. Netw.*, Rome, Italy, 2001, pp. 236–251.

[62] J. Kim, S. Kim, S. Choi, and D. Qiao, "CARA: Collision-aware rate adaptation for IEEE 802.11 WLANs," in *Proc. INFOCOM*, vol. 6, Barcelona, Spain, 2006, pp. 1–11.

[63] J. D. P. Pavon and S. Choi, "Link adaptation strategy for IEEE 802.11 WLAN via received signal strength measurement," in *Proc. IEEE Int. Conf. Commun. (ICC)*, vol. 2. Anchorage, AK, USA, 2003, pp. 1108–1113.

[64] P. Schramm, F. Müller, and H. G. Olofsson, "Cell selection in mobile radio systems," U.S. Patent 6 542 742 B2, Apr. 2003. [Online]. Available: https://www.google.com/patents/US6542742

[65] 3GPP. (Dec. 2011). *Protocol Specification; Radio Resource Control V.10.4.0*. [Online]. Available: http://www.3gpp.org/DynaReport/36331.htm

[66] R. Tanbourgi, S. Singh, J. G. Andrews, and F. K. Jondral "Analysis of non-coherent joint-transmission cooperation in heterogeneous cellular networks," in *Proc. IEEE Int. Commun. Conf. (ICC)*, Sydney, NSW, Australia, Jun. 2014, pp. 5160–5165.

[67] F. Guidolin, I. Pappalardo, A. Zanella, and M. Zorzi, "Context-aware handover in HetNets," in *Proc. Eur. Conf. Netw. Commun. (EuCNC)*, Bologna, Italy, Jun. 2014, pp. 1–5.

[68] F. Guidolin, I. Pappalardo, A. Zanella, and M. Zorzi, "A Markov-based framework for handover optimization in HetNets," in *Proc. IEEE IFIP Annu. Mediterr. Ad Hoc Netw. Workshop (Med-Hoc-Net)*, Piran, Slovenia, Jun. 2014, pp. 134–139.

[69] G. Shen, J. Liu, D. Wang, J. Wang, and S. Jin, "Multi-hop relay for next-generation wireless access networks," *Bell Labs Tech. J.*, vol. 13, no. 4, pp. 175–193, Dec. 2009.

[70] N. Sornin, M. Luis, T. Eirich, T. Kramp, and O. Hersent. (Jan. 2015). *LoRaWAN™ Specification*. Accessed on Feb. 21, 2016. [Online]. Available: https:// www.lora-alliance.org/portals/0/specs/LoRaWAN%20Specification%201R0.pdf

[71] L. Vangelista, A. Zanella, and M. Zorzi, "Long-range IoT technologies: The dawn of LoRa™," in *Future Access Enablers for Ubiquitous and Intelligent Infrastructures*. New York, NY, USA: Springer, 2015, pp. 51–58.

[72] C. Pielli, D. Zucchetto, A. A. Zanella, L. Vangelista, and M. Zorzi, "Platforms and protocols for the Internet of things," *EAI Endorsed Trans. Internet Things*, vol. 15, no. 1, Oct. 2015.

[73] C. Phillips, D. Sicker, and D. Grunwald, "A survey of wireless path loss prediction and coverage mapping methods," *IEEE Commun. Surveys Tuts.*, vol. 15, no. 1, pp. 255–270, Jan. 2013.

[74] S. Zvanovec, P. Pechac, and M. Klepal, "Wireless LAN networks design: Site survey or propagation modeling?' *Radioengineering*, vol. 12, no. 4, pp. 42–49, 2003.

[75] J. Koo and H. Cha, "Localizing WiFi access points using signal strength," *IEEE Commun. Lett.*, vol. 15, no. 2, pp. 187–189, Feb. 2011.

[76] M. Bocca, O. Kaltiokallio, and N. Patwari, "Radio tomographic imaging for ambient assisted living," in *Evaluating AAL Systems Through Competitive Benchmarking*. Heidelberg, Germany: Springer, 2012, pp. 108–130.

[77] B. Mager, "Fall detection using RF sensor networks," Ph.D. dissertation, Dept. Elect. Comput. Eng., Univ. Utah, Salt Lake City, UT, USA, 2013.

[78] A. Goldsmith, *Wireless Communications*. New York, NY, USA: Cambridge Univ. Press, 2005.

[79] M. D. Yacoub, "The α-μ distribution: A physical fading model for the Stacy distribution," *IEEE Trans. Veh. Technol.*, vol. 56, no. 1, pp. 27–34, Jan. 2007.

[80] CAS DataLoggers, Inc., *The Basics of Signal Attenuation*. Accessed on Feb. 21, 2016. [Online]. Available: https://www.dataloggerinc.com/content/files/whitepaper/wireless_data_loggers_accsense_temperature_datalogger.pdf

[81] P. Barsocchi, S. Lenzi, S. Chessa, and G. Giunta, "Virtual calibration for RSSI-based indoor localization with IEEE 802.15.4," in *Proc. IEEE Int. Conf. Commun. (ICC)*, Dresden, Germany, Jun. 2009, pp. 1–5.

[82] H. Hashemi, "The indoor radio propagation channel," *Proc. IEEE*, vol. 81, no. 7, pp. 943–968, Jul. 1993.

[83] N. Patwari, "Location estimation in sensor networks," M.S. thesis, Elect. Eng. Syst., Univ. Michigan, Ann Arbor, MI, USA, 2005.

[84] R. Crepaldi, A. F. Harris, A. Scarpa, A. Zanella, and M. Zorzi, "SignetLab: Deployable sensor network testbed and management tool," in *Proc. 4th ACM Int. Conf. Embedded Netw. Sensor Syst.*, Boulder, CO, USA, 2006, pp. 375–376.

[85] R. Crepaldi, P. Casari, A. Zanella, and M. Zorzi, "Testbed implementation and refinement of a range-based localization algorithm for wireless sensor networks," in *Proc. 3rd ACM Int. Conf. Mobile Technol. Appl. Syst.*, Bangkok, Thailand, 2006, Art. no. 61.

[86] R. Crepaldi *et al.*, "The design, deployment, and analysis of signetlab: A sensor network testbed and interactive management tool," in *Proc. IEEE Testbeds Res. Infrastruct. Develop. Netw. Commun. (TridentCom)*, Lake Buena Vista, FL, USA, 2007, pp. 1–10.

[87] R. Crepaldi, A. F. Harris, III, A. Zanella, and M. Zorzi, "SignetLab^2: A modular management architecture for wireless sensor networks," in *Proc. Wireless Commun. CNIT Thyrrenian Symp.*, 2007, pp. 331–345.
[88] Moteiv. *Tmote Sky: Ultra Low Power IEEE 802.15.4 Compliant Wireless Sensor Module*. Accessed on Apr. 26, 2016. [Online]. Available: http://www.eecs.harvard.edu/~konrad/projects/shimmer/references/tmote-sky-datasheet.pdf
[89] Chipcon Products From Texas Instruments. *CC2420: 2.4 GHz IEEE 802.15.4 / ZigBee-Ready RF Transceiver*. Accessed on Apr. 26, 2016. [Online]. Available: http://www.ti.com/lit/ds/symlink/cc2420.pdf
[90] *Cc1101 Low-Power Sub-1 GHz RF Transceiver: Data Sheet SWRS061G*, vol. 16, Texas Instruments, Dallas, TX, USA, 2011.
[91] Y. Chen and A. Terzis, "On the mechanisms and effects of calibrating RSSI measurements for 802.15.4 radios," in *Wireless Sensor Networks* (LNCS 5970), J. Silva, B. Krishnamachari, and F. Boavida, Eds. Heidelberg, Germany: Springer, 2010, pp. 256–271.
[92] S. Bolognani, S. D. Favero, L. Schenato, and D. Varagnolo, "Consensus-based distributed sensor calibration and least-square parameter identification in WSNs," *Int. J. Robust Nonlin. Control*, vol. 20, no. 2, pp. 176–193, Jan. 2010.
[93] A. Coluccia, "Reduced-bias ML-based estimators with low complexity for self-calibrating RSS ranging," *IEEE Trans. Wireless Commun.*, vol. 12, no. 3, pp. 1220–1230, Mar. 2013.
[94] H. Lim, L.-C. Kung, J. C. Hou, and H. Luo, "Zero-configuration indoor localization over IEEE 802.11 wireless infrastructure," *Wireless Netw.*, vol. 16, no. 2, pp. 405–420, 2010.
[95] H. Lim, L.-C. Kung, J. Hou, and H. Luo, "Zero-configuration, robust indoor localization: Theory and experimentation," in *Proc. IEEE Int. Conf. Comput. Commun. (INFOCOM)*, Barcelona, Spain, Apr. 2006, pp. 1–12.
[96] A. Zanella and A. Bardella, "RSS-based ranging by multichannel RSS averaging," *IEEE Wireless Commun. Lett.*, vol. 3, no. 1, pp. 10–13, Feb. 2014.
[97] A. Andersen, *Antenna Selection Guide SWRA161, Application Note AN058*, Texas Instruments, Dallas, TX, USA, 2007.
[98] D. Lymberopoulos, Q. Lindsey, and A. Savvides, "An empirical characterization of radio signal strength variability in 3-D IEEE 802.15.4 networks using monopole antennas," in *Wireless Sensor Networks* (LNCS 3868), K. Römer, H. Karl, and F. Mattern, Eds. Heidelberg, Germany: Springer, 2006, pp. 326–341.
[99] A. A. M. Saleh and R. Valenzuela, "A statistical model for indoor multipath propagation," *IEEE J. Sel. Areas Commun.*, vol. 5, no. 2, pp. 128–137, Feb. 1987.
[100] J. Ø. Nielsen, V. Afanassiev, and J. B. Andersen, "A dynamic model of the indoor channel," *Wireless Pers. Commun.*, vol. 19, no. 2, pp. 91–120, 2001.
[101] N. H. Shepherd, "Radio wave loss deviation and shadow loss at 900 MHz," in *Proc. IEEE 26th Veh. Technol. Conf.*, vol. 26. Washington, DC, USA, Mar. 1976, pp. 63–66.
[102] F. Babich, G. Lombardi, L. Tomasi, and E. Valentinuzzi, "Indoor propagation measurements at DECT frequencies," in *Proc. Mediterr. Electrotech. Conf. (MELECON)*, vol. 3. Bari, Italy, May 1996, pp. 1355–1359.
[103] G. Tzeremes and C. G. Christodoulou, "Use of Weibull distribution for describing outdoor multipath fading," in *Proc. IEEE Antennas Propag. Soc. Int. Symp.*, vol. 1. San Antonio, TX, USA, 2002, pp. 232–235.
[104] Y. Zhao, Y. Liu, T. He, A. V. Vasilakos, and C. Hu, "FREDI: Robust RSS-based ranging with multipath effect and radio interference," in *Proc. IEEE INFOCOM*, Turin, Italy, 2013, pp. 505–509.
[105] D. Zhang, Y. Liu, X. Guo, M. Gao, and L. M. Ni, "On distinguishing the multiple radio paths in RSS-based ranging," in *Proc. IEEE INFOCOM*, Orlando, FL, USA, 2012, pp. 2201–2209.
[106] H. MacLeod, C. Loadman, and Z. Chen, "Experimental studies of the 2.4-GHz ISM wireless indoor channel," in *Proc. 3rd Annu. Commun. Netw. Services Res. Conf.*, Halifax, NS, Canada, May 2005, pp. 63–68.
[107] H.-J. Zepernick and T. A. Wysocki, "Multipath channel parameters for the indoor radio at 2.4 GHz ISM band," in *Proc. IEEE Veh. Technol. Conf. (VTC)*, vol. 1. Houston, TX, USA, Jul. 1999, pp. 190–193.
[108] A. J. Coulson, A. G. Williamson, and R. G.Vaughan, "Improved fading distribution for mobile radio," *IEE Proc. Commun.*, vol. 145, no. 3, pp. 197–202, Jun. 1998.
[109] S. Buyukcorak, M. Vural, and G. K. Kurt, "Lognormal mixture shadowing," *IEEE Trans. Veh. Technol.*, vol. 64, no. 10, pp. 4386–4398, Oct. 2015.
[110] R. Parasuraman, S. Caccamo, F. Baberg, and P. Ogren. (Jan. 2016). *CRAWDAD Dataset KTH/RSS (V. 2016-01-05) Traceset: Outdoor*. [Online]. Available: http://crawdad.org/kth/rss/20160105/outdoor
[111] H. D. Hristov, *Fresnal Zones in Wireless Links, Zone Plate Lenses and Antennas*, 1st ed. Norwood, MA, USA: Artech House, Inc., 2000.
[112] Z. Xiao *et al.*, "Non-line-of-sight identification and mitigation using received signal strength," *IEEE Trans. Wireless Commun.*, vol. 14, no. 3, pp. 1689–1702, Mar. 2015.
[113] P.-C. Chen, "A non-line-of-sight error mitigation algorithm in location estimation," in *Proc. Wireless Commun. Netw. Conf. (WCNC)*, New Orleans, LA, USA, 1999, pp. 316–320.
[114] C. A. Boano, N. Tsiftes, T. Voigt, J. Brown, and U. Roedig, "The impact of temperature on outdoor industrial sensornet applications," *IEEE Trans. Ind. Informat.*, vol. 6, no. 3, pp. 451–459, Aug. 2010.
[115] F. Bandiera, A. Coluccia, G. Ricci, and A. Toma, "RSS-based localization in non-homogeneous environments," in *Proc. IEEE Int. Conf. Acoust. Speech Signal Process. (ICASSP)*, Florence, Italy, May 2014, pp. 4214–4218.
[116] A. Coluccia and F. Ricciato, "RSS-based localization via Bayesian ranging and iterative least squares positioning," *IEEE Commun. Lett.*, vol. 18, no. 5, pp. 873–876, May 2014.
[117] C.-H. Chen and K.-T. Feng, "Enhanced distance and location estimation for broadband wireless networks," *IEEE Trans. Mobile Comput.*, vol. 14, no. 11, pp. 2257–2271, Nov. 2015.
[118] F. Xia, X. Yang, H. Liu, Z. Da, and W. Zhao, "Energy-efficient opportunistic localization with indoor wireless sensor networks," *Comput. Sci. Inf. Syst.*, vol. 8, no. 4, pp. 973–990, 2011.
[119] F. Zorzi and A. Zanella, "Opportunistic localization: Modeling and analysis," in *Proc. IEEE Veh. Technol. Conf. (VTC)*, Barcelona, Spain, 2009, pp. 1–5.
[120] E. Gonendik and S. Gezici, "Fundamental limits on RSS based range estimation in visible light positioning systems," *IEEE Commun. Lett.*, vol. 19, no. 12, pp. 2138–2141, Dec. 2015.
[121] A. Zanella, N. Bui, A. Castellani, L. Vangelista, and M. Zorzi, "Internet of things for smart cities," *IEEE Internet Things J.*, vol. 1, no. 1, pp. 22–32, Feb. 2014.

Andrea Zanella (S'98–M'01–SM'13) received the Laurea degree in computer engineering, and the Ph.D. degree in telecommunications engineering from the University of Padova, Italy, in 1998 and 2001, respectively. He was a Visiting Scholar with the Department of Computer Science, University of California, Los Angeles (UCLA), in 2000. He is currently an Associate Professor with the Department of Information Engineering, University of Padova. He is one of the coordinators of the SIGnals and NETworking Research Laboratory. His long-established research activities are in the fields of protocol design, optimization, and performance evaluation of wired and wireless networks. He is currently an Associate Editor of the IEEE TRANSACTIONS ON COGNITIVE COMMUNICATIONS AND NETWORKING and the IEEE INTERNET OF THINGS JOURNAL. He previously served as an Editor for *Digital Communications and Networks*.